HELLENIC REPUBLIC
National and Kapodistrian University of Athens
EST. 1837

School of Health Sciences
School of Medicine and Department of Pharmacy

Interdisciplinary Postgraduate Studies Program in

Nanomedicine

Mixed copolymer-based micelles for the encapsulation of hydrophobic drugs

Gerardou Angeliki Maria

Chemist

Supervised by

Dr. Asterios (Stergios) Pispas

Thesis committee members

Dr. Natassa Pippa

Dr. Costas Demetzos

August 2022

Acknowledgments

First of all, I would like to express my very great appreciation to my supervisor Stergios Pispas, for his invaluable guidance, feedback, and overall insights in this field that have made this project an inspiring experience for me. I would also like to extend my deepest gratitude to my committee, Dr. Natassa Pippa and Dr. Costas Demetzos who generously provided knowledge and expertise. This endeavor would not have been possible without Ph.D. candidate Anastasia Balafouti who was always there to discuss anything I was unsure of. I want to give my deepest appreciation to the rest of the team, Postdoctoral researchers Maria Karayianni and Angeliki Chroni, Ph.D. candidates Varvara Chrisostomou, Antiopi Vardaxi, and Dimitris Selianitis, and Master student Dimitris Vagenas for the constant encouragement and for making me feel part of the group from day one. Words cannot express my gratitude to my parents Judy and Kostas for supporting me and to whom I owe my love for knowledge.

Table of Contents

Table of Figures

List of Tables

Abstract

Current drug development is seeing an increase in the number of lipophilic drug candidates with limited water solubility. A large number of novel drugs are rejected in the early stages of research due to their poor water solubility, making it a key issue in today's biopharmaceutics. Low solubility is almost always coupled with low bioavailability. To avoid missing out on promising medication prospects, it is crucial to establish innovative formulation systems to make these compounds bioavailable.[1–3] Nanotechnology appears to have found a solution, utilizing mixed copolymer-based micelles for targeted drug delivery. Mixed micelles offer a plethora of advantages with little to no effort in synthesis.[4] It is for this reason that the focus of this study is on the numerous strategies for forming and stabilizing mixed micelles for drug delivery of two active pharmaceutical ingredients exhibiting different degrees of solubility.

In our research, various synthetic routes will be taken to obtain mixed micelles combining hyperbranched H-[poly (ethylene glycol) methyl ether methacrylate-co-lauryl methacrylate], H-[P(OEGMA-co-LMA)] copolymer and Pluronic F_{127} triblock copolymer[5]. The combination of these biocompatible copolymers into mixed nanostructures will be studied thoroughly with or without the encapsulation of model hydrophobic drugs, namely curcumin and indomethacin. Different physicochemical techniques, including light scattering methods (DLS, ELS), UV-Vis, and fluorescence spectroscopy (FS) are utilized to assess features, such as the size, the homogeneity, and surface charge of the emerged nanostructures in aqueous media and furthermore evaluate their potential use as nanocarriers. Results indicated that the copolymers combined, spontaneously self-assemble into mixed micelles in aqueous media, whereas both systems of empty and drug-loaded micelles exhibit favorable features, such as small average micelle hydrodynamic radius and low-size polydispersity indexes.

Keywords: Drug encapsulation, mixed micelles, curcumin, indomethacin, bioimaging, poloxamers, hyperbranched copolymers.

Introduction

1.1 Amphiphilic polymers

Referred to often also as macromolecules, polymers are chains of compounds in which each compound could be a bead on a string and each bead is a monomeric unit. There are naturally occurring polymers such as rubber and synthetic such as polystyrene. The structure of these polymers is comprised of several molecular units connected by covalent bonds. In the case there is only one monomeric unit repeating itself, it is described as a homopolymer. Otherwise, it is referred to as a copolymer. To be exact, if there is a specific pattern transpiring among the units, it is classified as a block copolymer, if not, as is in this incident, random copolymers are formed.[6,7] Blocks or segments of opposing philicity, hydrophilic and hydrophobic, make up amphiphilic copolymers. The percentage of each affects their self-assembly in an aqueous solution and frequently leads to the development of aggregates such as micelles. Modifying the size and shape of amphiphilic polymers various morphologies can be obtained, making them ideal candidates for biomedical applications.[8,9]

1.1.2 Triblock copolymers

In the event, three separate polymer segments, A, B, and C, are joined by covalent bonds ABC triblock copolymers are formed[10]. Also, when three separate monomeric units, rather than two, are joined together to produce an ABC triblock copolymer, the structural variation goes up dramatically and, in some cases, ABC copolymers can create morphologies not possible with AB copolymers, such as raspberry forms. The third block contributes a greater degree of complexity and flexibility.[11,12] Triblock copolymers with two types of copolymers (A, hydrophobic polymer, and B, hydrophilic polymer), can also be categorized as symmetric ABA and BAB triblock copolymers.[13]

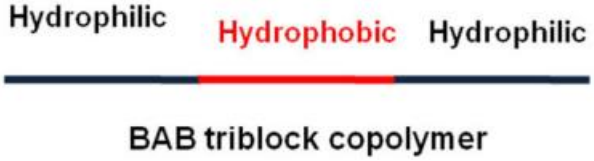

Figure 1. A depiction of a symmetric triblock copolymer [13]

1.1.3 Hyperbranched Polymers

Highly branched macromolecules exhibiting a three-dimensional dendritic-like structure are known as hyperbranched polymers. Inspired by the Greek word dendron, these tree-like polymers offer a multitude of advantages. For example, in comparison to their similarly structured polymers, dendrimers, hyperbranched polymer's ease of synthesis could lead to affordable production on a greater scale to succeed commercially since no protection/deprotection steps are necessary. This is because certain linearly integrated A_xB monomers are permitted in hyperbranched polymers. This feature is an easy way to distinguish dendrimers and hyperbranched polymers, strictly speaking, the proportion of branched, terminal, and linear units in the polymer structure (also known as the "branching factor) for dendrimers is 100%. This contrasts with hyperbranched structures where the ratio is below 100%. Additionally, contrary to traditional linear polymers, the abundance of functional groups allows for greater customization and the nature of end groups greatly influences features, such as glass transition temperature, solubility, and viscosity.[14–17]

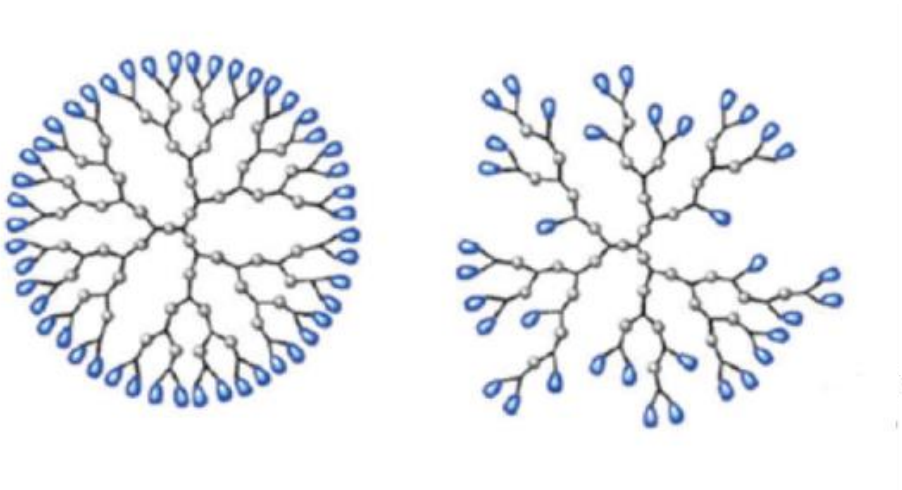

Figure 2. Members of the dendritic family. A dendrimer (on the left) and a hyperbranched polymer (on the right).[18]

1.1.4 H-[P(OEGMA-co-LMA)] 50%w/w LMA and RAFT polymerization.

H-[P(OEGMA-co-LMA)], the hyperbranched polymer, was synthesized via Reversible Addition Fragmentation Chain-transfer Polymerization, containing diester ethylene glycol dimethacrylate (EGDMA) as the branching agent and was kindly provided by Ph.D. candidate Anastasia Balafouti. The RAFT process has become a well-known polymerization technique that has gained acceptance outside of polymer research as a means of producing materials with a wide range of uses, from materials science to medicine.[19] RAFT is a type of controlled radical polymerization. A characteristic much needed for medical applications

to avoid disparities such as heterogeneity in chain lengths and other features which could lead to a sub-par product. A RAFT polymerization system comprises a solvent, a RAFT agent, a monomer, and an initiator. The reaction is set in motion by radical initiators, for instance, AIBN. Radicals are produced through fragmentation of the initiator, which then combines with monomer molecules to produce propagating radicals Pm• which launches an active polymerizing chain. The active chains (Pm) which were generated in the initiation stage react with the RAFT agent generating, as result, the leaving group (R•). In this reversible phase, intermediate species have the potential to either fragment to produce an oligomeric RAFT agent and an R radical or otherwise fragment back to the original RAFT agent and a radical species R. Reinitiation takes place when a monomer species reacts with the leaving group radical to construct a separate active polymer chain. The procedures of addition-fragmentation or equilibration are then applied to this active chain (Pn•). The majority of the active propagating species are trapped in the dormant thiocarbonyl molecule during equilibration, a crucial phase in the RAFT process. The likelihood of chain termination is thus reduced. Pm• and Pn•, active polymer radicals, are balanced between the active and dormant states. A polymer chain is engaged in polymerization while another is inactive being attached to the thioester molecule. Despite being few in number, termination reactions nonetheless happen as a result of combination or disproportionation mechanisms.[20–22]

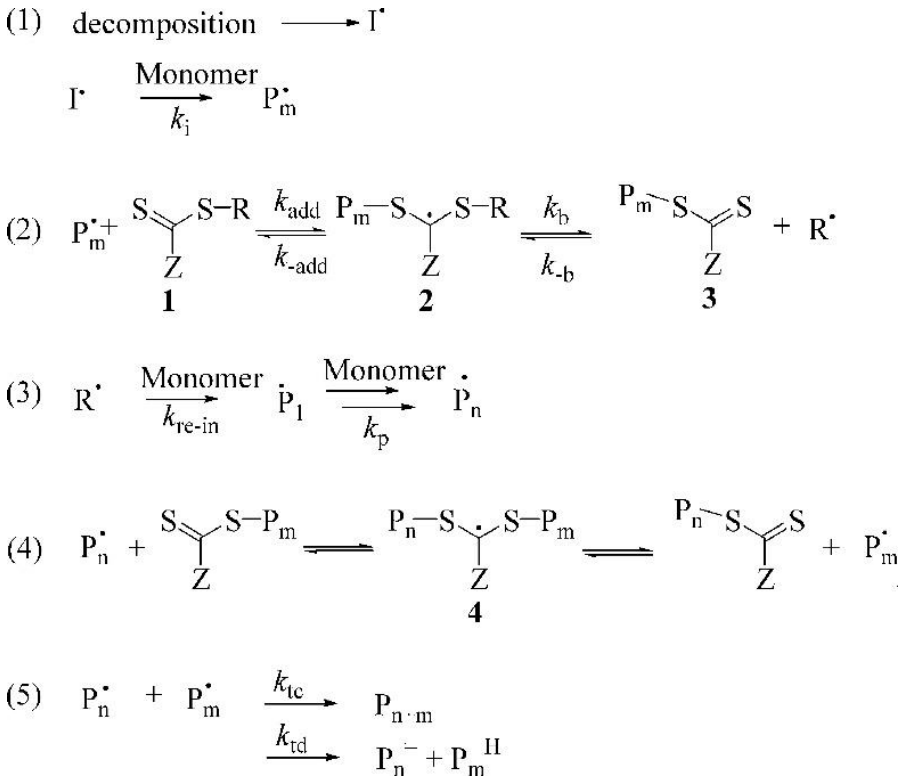

Figure 3. A scheme of the RAFT Polymerization mechanisms.[22]

Oligo (ethylene glycol) - methyl ether methacrylate (OEGMA) and lauryl methacrylate (LMA) are biocompatible monomers, while their polymers are highly hydrophilic and

hydrophobic respectively. OEGMA is a PEG analog commonly investigated as a coating for synthetic polymeric nanoparticles in the field of biotechnology. Due to its biodegradability and simple functionalization, hydrophobic LMA has garnered increasing interest. PLMA has been utilized in some medical research, including targeted drug delivery, cell labeling, and tissue engineering.[23,24]

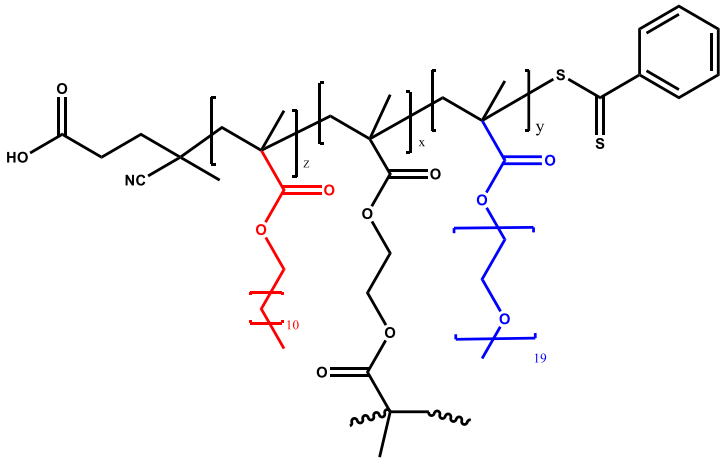

Figure 4. H-[P(OEGMA-co-LMA)]

1.1.5 Pluronics and thermosensitive polymers

Polymers exhibiting thermosensitive properties constitute a significant type of stimuli-responsive drug delivery methods and have received a great amount of attention in the past century, especially in the realm of controlled drug release. To clarify, an optimum controlled drug delivery system, distributes the A.P.I. for a predetermined amount of time, topically or systematically. These thermosensitive polymers allow the formulation to be administered as a liquid at room temperature, which gels at body temperature. When compared to other existing drug delivery systems, thermosensitive micelles are known to extend the circulation time while maintaining the stability of sensitive biomolecules e.g., proteins. A temperature-induced reversible gel-sol transition can occur with several commonly available block copolymers, including Pluronic F127 and other poloxamers, when the system goes through a temperature shift. Owing to their widespread availability in a variety of molecular weights and block ratios, these systems have been extensively investigated. These water-soluble and low-toxic, PEO-PPO-PEO copolymers are made of poly(propylene oxide), and poly(ethylene oxide) which is commercially known as PEG. Among the most popular of these copolymers is Pluronic F127, which has a molecular weight of 12.500 and consists of a PPO block at its center and PEO surrounding it at a ratio of 2:1 by weight. As temperatures rise the PPO blocks become more and more hydrophobic and start to agglomerate. This characteristic allows the sustained release from the application site, the release of the encapsulated drug from its core. Notably, Pluronic F127 has been authorized by the Food and Drug Administration (FDA) for several medical applications, including drug delivery. When a hydrophobic drug is combined with an

adequate amount of Pluronic in an aqueous media and the temperature is increased to 37°C, the drug molecules tend to gather in the hydrophobic PPO cores. The PEO units make up a corona shielding the hydrophobic drug which is gravitating towards the core and keeps it intact for a certain period. As a result, the hydrophobic drug's water solubility drastically improves in aqueous solutions, boosting the A.P.I.'s bioavailability. An interesting take has been if the hydrophobic drug will affect the size of the emerged nanocarrier. There was a modest decrease in micelle size according to a study where indomethacin was encapsulated in a polymeric micelle. It must be said that although most Poloxamers are typically incompetent to biodegrade just as many other nano-scaled molecules they are eliminated through urine.[25–35]

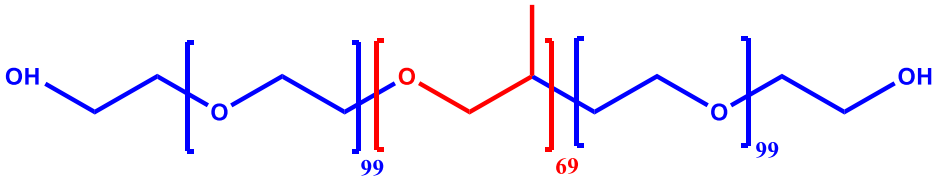

Figure 5. Pluronic F127.

1.1.6 Polymeric micelles – Drug delivery

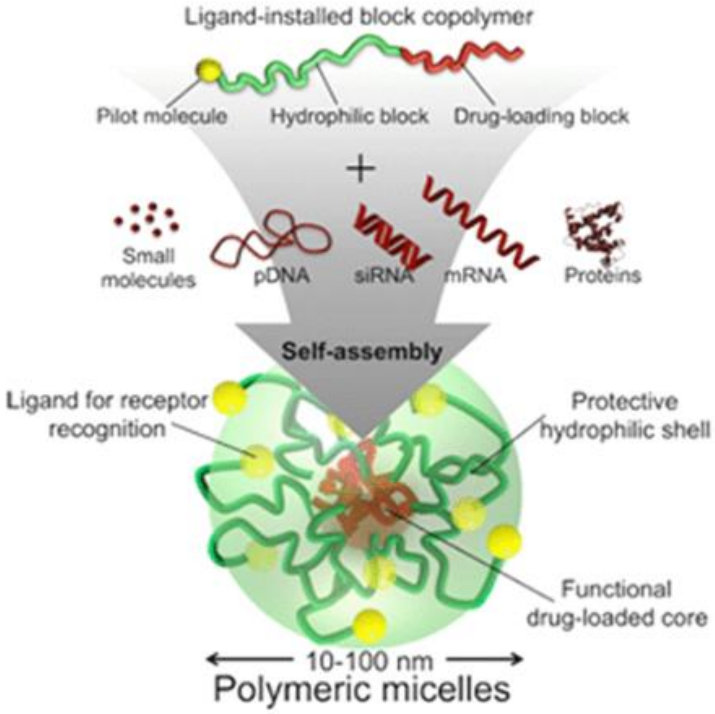

Figure 6. A depiction of some key components in the formation of a polymeric micelle[36]

Amphiphilic copolymers tend to self-assemble into polymeric micelles in an aqueous environment. The structure of polymeric micelles can be categorized into two distinct sections, a drug-loading center which serves as a micro reservoir for the encapsulation of hydrophobic drugs and biomolecules, for instance, DNA; and a hydrophilic exterior that can interact with the biological environment, once exposed. They are mostly spherical in shape and due to the ease of modifications, they enable the creation of specialized nanocarriers that can be specifically produced in consideration of the disease pathogenesis, the method and site of administration, and other factors. The ability of micelles to encapsulate drugs is largely dictated by the length of hydrophobic units and the type of functional groups present in the core. To explain further, hydrophobic drugs are mostly drawn into the micelle either by covalent bonding with the chains of the hydrophobic region or by hydrophobic interactions. To illustrate, in the case of a negatively charged biomolecule such as an amino acid, oppositely charged units are employed to create polyion complex (PIC) cores via electrostatic interactions. Improvement in nanocarrier durability and regulation of drug release also may be achieved by altering the chemical structure of polymeric micelles.

To sum up and reiterate polymeric micelles have a number of fundamental qualities that make them ideal for use in drug delivery:

- A biocompatible corona to minimize the interactions with the reticuloendothelial system (RES), which is part of our immune system, primarily monocytes, and macrophages that are mostly found in the liver and spleen. To avoid, as long as feasible, phagocytosis will result in extending the circulation time of the nanocarrier. Additionally, “stealthiness” is often achieved by PEGylation.
- A hydrophilic coating surrounding a hydrophobic drug-loading core that enables the solubilization of hydrophobic drugs and protects the precious cargo from degradation before it reaches its target. Polyethylene glycol (PEG) or commonly referred to as polyethylene oxide in chemistry journals is a hydrophilic polymer used in myriad nanocarrier applications as a protective barrier.[37–42]
- A size in the optimal range of the nanoscale to prevent swift renal excretion, allowing accumulation inside tumor tissues or any other target via the EPR effect. The EPR effect is a form of passive targeting utilized by nanoparticles. The permeability of the tumor vessels, which allows particles to penetrate the cavities of the tumor, but also the absence of lymphatic drainage within the tumor area, enables them to remain within and therefore avoid being "flushed" out. In contrast to the gaps of the regular vessel wall, which are fewer than 10 nm in size, these perforations might be even in the range of over 200 nm in the case of a cancerous tumor.[43,44] This leads to the conclusion polymeric micelles will avoid healthy tissues. It ought to be mentioned that a nanoparticle should not be excessively small. As the cutoff for rapid renal excretion in the kidneys is roughly 6 nm, anything larger than this limit will result in a prolongation of the polymeric micelle’s half-life. Although academics do not always agree, the happy medium is generally thought to lie

between 10 and 100 nm. Following the sinking phenomena, bigger structures have a tendency to accumulate in the liver and spleen.

- Stimuli-sensitive properties. By utilizing pH-sensitive polymers we can increase polymeric micelle's selectivity for malignant tissues. The environment around tumors is acidic, with a pH spectrum of 6.5 to 7.0. Limiting the drug's release to this location solely to prevent it from being burst in blood circulation. The pH declines inside endosomal chambers, even on a subcellular level that results in a pH value of 5.5, serves as a specific trigger for controlled drug release.[36]

Various routes may be taken to encapsulate a drug in a micellar system:

- In the dialysis method, the copolymers, and the A.P.I. are dispersed in a water-miscible organic solvent (that could combine with water and form a homogenous solution e.g., ethanol) and left to be dialyzed in water. The gradual replacement of the organic solvent triggers the formation of micelles. The dialysis tubing allows the unloaded drug to move freely yet prevents the polymeric micelles from escaping.
- The oil/water emulsion approach involves first dispersing the copolymers in an aqueous solution, then, after dissolving the drug in a volatile organic solvent, the organic phase is added to the aqueous phase while vigorously stirring. As the solvent evaporates, the drug-loaded polymeric micelles are formed.
- The solvent evaporation method, often referred to as the thin film hydration method relies on dissolving the drug and polymer in a volatile organic solvent and then allowing the solvent to completely evaporate by vacuum or with heat. The emerged thin film is rehydrated with or without sonication or simply stirring.
- With the co-solvent evaporation approach, both polymer and drug are dispersed in a volatile water-miscible organic solvent. Then water or phosphate buffer solution is introduced to the organic phase or the other way around, therefore initiating self-assembly and drug entrapment. The organic co-solvent is then evaporated by heat.[38–42]

1.1.7 Polymeric micelles in Bioimaging

As early detection and therapy are key for many pathological states, nanotechnology seems to have found the solution with the creation of screening methods that make it possible to identify a variety of abnormalities in minuscule amounts. Therefore, it is reasonable for diagnostic methods, such as fluorescence imaging (FI), to take advantage of the opportunity nanoparticles offer. While it is nothing new, interest has grown in this form of imaging due to the use of novel probes. Already being sensitive, selective, contrast-rich, and adaptable as an imaging technique, fluorescent nanoparticles only elevate the end result. Although the use of organic dyes and other standard probes often exhibit acceptable biocompatibility and small size, they lack targeting mechanisms, and most times suffer from low absorption, leading to swift expulsion from the body. On the other hand, fluorescent nanoparticles are essentially inert. They barely interact with cellular proteins

and are unaffected in terms of their optical properties. Predictably, the photostability properties of nanoparticles are noticeably superior in comparison to those of molecular probes. Furthermore, in the case of passive targeting, as the form of distribution of nanoparticles, they are spread more uniformly throughout the body. Additionally, especially with polymeric nanocarriers, there is the possibility of loading numerous contrasting agents to be able to utilize various methods of imaging stimulatingly. These systems are fairly simple to modify, especially with the increase in real estate which is offered with polymers with multiple functional groups that could take part in interactions with the environment and the target. To reiterate, amphiphilic polymers offer the ability to modify the ratio of hydrophobic/hydrophilic copolymers.[45–49]

1.1.8. Mixed polymeric micelles

Polymeric micelles which are derived from one type of copolymer may exhibit insufficiency in certain aspects. Given that these micelles are hampered by the fact that they possess a limited quantity of building blocks (colloquially known as units). To overcome these hurdles, a tried-and-true method is by combining a number of distinct amphiphilic polymers to produce mixed micelles. There is potential to improve the existing optimal features and get around some of the emerging drawbacks of conventional polymeric micelles with little to no effort regarding synthetic procedures. Research has shown time and again, that mixed micelles offer substantial gains:

- in thermodynamics with the decrease of critical micelle concentration (more on this can be found in the corresponding chapter 4.1.2).
- in micelle durability by boosting the hydrophobic interactions, H-bonding, and other stabilizing factors.
- in drug entrapment efficiency by increasing capacity.
- in controlling the size of the emerged nanoparticles.
- in the ease to add multiple features (e.g., thermosensitive capabilities).

As all the above points have demonstrated, mixed micelles often manage to outperform typical polymeric micelles. One will find several factors which play a key role to obtain mixed micelles to list a few:

- Hydrophobic interactions are the utmost widely researched form of stabilizing properties in mixed systems. In a nutshell, this form of non-covalent interaction is based on the interplay between the hydrophobic and hydrophilic units of the copolymers. Poloxamers are a major group of copolymers that utilizes this form of stabilization and are added to nanocarrier formulations. This is often the case because of some shortcomings which could arise in conventional micelles, including their incapacity to incorporate significant amounts of hydrophobic drugs and their high critical micelle concentrations (CMC), which cause poor

micelle stability and rupture when diluted in circulation following intravenous administration. Mixing with a more hydrophobic copolymer may considerably enhance the longevity of the emerging micelles and hence the bioavailability of the encapsulated drugs. Isothermal titration calorimetry (ITC) analysis at various temperatures can be used to investigate the hydrophobic interactions within the micelles. ITC analysis is habitually utilized in block copolymer mixed micelles with surfactants but has not yet been conducted on mixed micelles derived from block copolymers. In essence, the premise is that temperature is the most principal factor influencing hydrophobic interactions because, as temperatures rise, hydrophobic interactions tend to increase. The increase can be mapped onto the differential enthalpy curves of the ITC analysis, demonstrating that hydrophobic interactions are the driving factor in the micellization of two polymers. It should be noted that, although ITC analysis is beneficial for confirming hydrophobic interactions, another method is necessary to analyze the development of mixed systems.

- Hydrogen bonds are short-range interactions that develop solely when the two functional groups are in close vicinity to one another. It is presumed that two separate amphiphilic copolymers self-assemble to form micellar systems, initially as a direct consequence of the interactions of the hydrophobic blocks with the aqueous media, and afterward, hydrogen bonds form when the functional groups in the two copolymers' hydrophobic blocks come close to each other, stabilizing the hydrophobic core. FT-IR spectra may be employed to determine hydrogen bonds between specific hydrogen bond acceptors and donors in the different units of the copolymers if there is a drop in the peak frequency of the bands to a lower wavenumber.
- Ionic bonds, these long-distance interactions are centered on the strong electrostatic affinity between a pair of oppositely charged copolymers. This kind of mixed micelle is classified as a polyion complex (PIC) micelle. When copolymers are dispersed in water, their oppositely charged units come together to create aggregates, which in turn trigger the production of mixed micelles. In contrast to the conventional mixed micelles generated by formerly listed interactions, PIC micelles offer the extra benefit of encapsulating ionic substances much like plasmid DNA. PH influences the stability of PIC micelles. To clarify the basic that is the positively charged unit gets less ionized and eventually neutral as pH climbs. In the same vein, as pH falls, the acidic, which is the negatively charged unit, becomes less ionized through protonation. In brief, pH fluctuations in the PIC micelle system induce a decrease in electrostatic interactions between the various copolymers, while hydrophobic interactions gain prominence in micelle assembly.[35,50–53]

1.2 Curcumin

Curcumin is the most prevalent polyphenolic compound in turmeric. It is extracted from the rhizome of turmeric, a perennial plant with the botanical name, Curcuma longa. Turmeric has a long history in Asian countries as a seasoning, a pigment, and in medicine. Even as early as 1280, Marco Polo mentions turmeric in his excursion chronicles about China and India. Fast forward to now, turmeric is still in use today in textiles and as a culinary pigment for food chemistry applications. Just as previously stated, the use of curcumin in medicine is not something new. Considering this, researchers have intensively explored curcumin's potential. Studies have documented a broad range of therapeutic applications such as antioxidant, anti-inflammatory, and anti-tumor activity, anti-microbial, anti-protein aggregation, and wound healing capabilities.

Taking into consideration the above, curcumin seems to possess both preventive and therapeutic effects in cancer, atherosclerosis, aging, and neurodegenerative disorders by regulating various molecular targets. We must keep in mind that the aqueous solubility of curcumin is limited; therefore, it is substantially restricted in its availability and is swiftly removed through the gallbladder after being metabolized in the liver. These are both key hurdles in employing it for disease therapy. Curcumin degrades quickly, first via hydrolysis, then through molecular fragmentation. Drug nanoformulation in polymeric micelles has been increasingly explored to address the aforementioned curcumin challenges. As previously mentioned, polymeric micelles are thought to be one of the most effective methods for delivering poorly soluble drugs such as curcumin. In addition to mixed micelles attributes many studies have come forward, utilizing Pluronic copolymers such as mixed micelles composed of P123 -F68 and F127 - F68. In both cases, this type of nanoformulation may be a promising delivery system.[35,54–60]

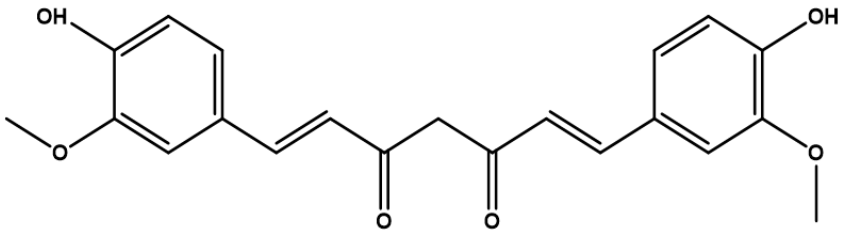

Figure 7. Chemical structure of curcumin.

1.3 Indomethacin

Indomethacin, also known as 1-(4-chlorobenzoyl)-5-methoxy-2-methylindole-3-acetic acid, is a powerful nonsteroidal anti-inflammatory drug (NSAID). Indomethacin is a drug that is widely used to relieve pain, fever, edema, stiffness, and tenderness. These properties are the reason indomethacin has a vital role in the treatment of osteoarthritis, rheumatoid

arthritis, tendinitis pain, migraines, menstrual cramping, and connective tissue diseases. Indomethacin operates by inhibiting cyclooxygenase enzyme (COX-1 and COX-2) activity and hence suppressing prostaglandin synthesis in the tissues. Indomethacin also exhibits a significant tocolytic effect. It is also associated with some adverse implications though, including gastrointestinal mucosal irritation after oral administration and central nervous system toxicity (e.g., confusion) as an inevitable result of high plasma levels. Roughly 30-60% of people receiving standard therapeutic doses of this drug develop side effects, with 10-20% quitting treatment. In conjunction with the moderate hydrophobicity indomethacin exhibits, it is a perfect candidate for mixed micelles. A good example is a thermo-sensitive chitosan-Pluronic copolymer nanosystem which successfully encapsulated indomethacin and demonstrated favorable results as a drug carrier for sustained delivery. In a similar fashion amphiphilic polyphosphazenes incorporated indomethacin and achieved prolonged retention in circulation in comparison to the free drug.[61–66]

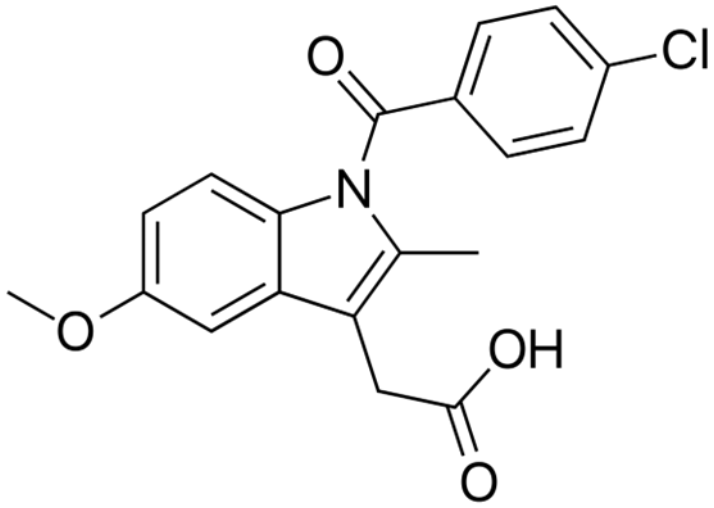

Figure 8. Chemical structure of indomethacin.

Materials and Methods

2. Materials

Pluronic F127 was purchased from Sigma (Athens, Greece), Hyperbranched copolymer H-[P(OEGMA-co-LMA)] 50%w/w LMA was provided by Ph.D. candidate Anastasia Balafouti, curcumin was purchased from Merk, indomethacin was procured from Sigma-Aldrich

(Athens, Greece). Fetal Bovine Serum and phosphate-buffered saline tablets (PBS, 98%) were acquired from Sigma -Aldrich (Athens, Greece).

2.1. Mixed Micelles Preparation

2.1.1 Preparation of blank mixed micelles

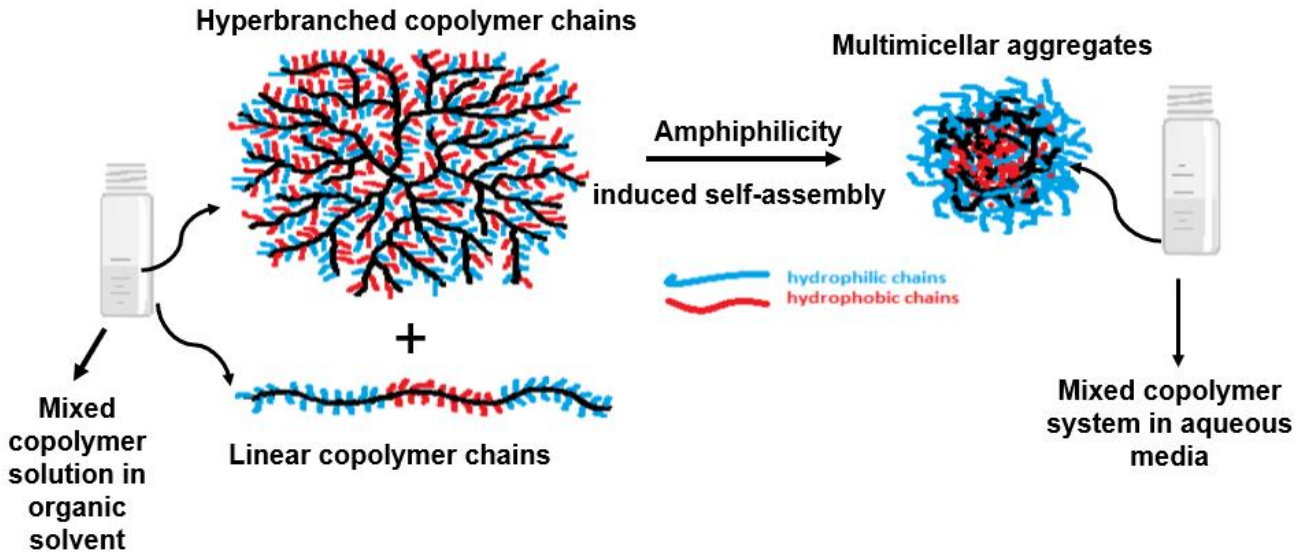

Figure 9. Schematic representation of the formation of mixed micelles.

Various routes were taken to obtain the emerged nanostructures. The synthetic procedure of H-[P(OEGMA-co-LMA)] can be found in citation 23. The thin film method and the co-solvent evaporation approach were utilized to produce neat nanostructures.

Thin film method

1. Quantities were weighed in 12 mL vials which were swiftly capped to avoid contamination. 0.005g of H-[P(OEGMA-co-LMA)] and 0.005g (or 0.01g depending on the ratio needed) of Pluronic F127 were initially dissolved separately in ethanol (this solvent was used only in 1_H:1_{F127} ratio). To clarify, one solvent was chosen for each protocol to dissolve each copolymer. Each sample was left to rest for 10 min, starting the clock after there was no sign of undissolved polymers. Some heat was required to dissolve the triblock copolymer in all cases. For all polymers, 0.5 mL ethanol was used. For the hyperbranched copolymer, only 0.5 mL acetone was utilized. Likewise, in the case of Pluronic, it was dissolved in 0.5mL with the

exception of the 0.01g quantity in which 1.5 mL of acetone was needed to dissolve the copolymer.

2. The copolymers were then mixed at the desired ratio. Each sample was left for at least an hour to rest.
3. The systems were then transferred to separate round bottom flasks to obtain the different copolymer ratios. The volatile solvent was evaporated by rotary evaporation at room temperature for about 1 hour depending on the solvent until a clear film was formed on the inner wall of the flask.
4. The film was then rehydrated with 5 mL of Phosphate Buffer Saline (pH:7.3) agitating the walls of the flask. The emerged colloidal systems were then transferred to a 12mL vial and left to stand for 24 hours before characterization. The final concentration of H-[P(OEGMA-co-LMA)] in all colloidal systems was 10^{-3} g/mL.

The co-solvent evaporation approach

1. 0.005g of H-[P(OEGMA-co-LMA)] and 0,005g (or 0,01g based upon the required ratio) of Pluronic F127 were weighed in 12 mL vials and were first dissolved individually in the ethanol or acetone depending on the protocol. Samples were allowed to settle for 10 minutes once there was no indication of undissolved polymers. In all cases, warmth from our hands was required to dissolve Pluronic F127. The same amounts of organic solvent were employed, apart from 0.01g Pluronic, which required 3 mL of ethanol to dissolve.
2. Afterwards, the copolymers were combined at the appropriate ratio. Each sample was allowed to rest overnight.
3. The newly constituted mixed samples were then injected into 5mL of “water for injection” or buffer solution (pH:7.3) in agitation. For mixing purposes, a magnetic stirrer was utilized. This step was carried out for approximately 3 min or until all signs of cloudiness had disappeared. Tall vials were utilized for practical reasons at this step.
4. Heat was applied to the system with the use of a water bath and magnetic mixer- hot plate until the solvent evaporated. Samples were heated above the boiling point of the organic solvent. Heating time varied and was determined by the amount of solvent. After the samples cooled down, they were capped and set aside to be characterized the following day. The final concentration of H-[P(OEGMA-co-LMA)] in all colloidal systems was 10^{-3} g/mL.

2.1.2 Preparation of drug-loaded micelles

Taking into consideration both copolymers’ biocompatibility and self-assembling behavior, curcumin and indomethacin encapsulation ability was investigated. The systems were prepared at 10^{-3} g/mL hyperbranched copolymer concentration. The theoretical

encapsulation degree of each drug was relative to both copolymers and the two formulations of curcumin were calculated by summing up the weight ratio to 10% and 20% and for indomethacin 10%. The co-solvent evaporation approach was used to prepare the drug-loaded mixed micelles. In a similar manner, following step 2 of the co-solvent evaporation approach, curcumin and indomethacin stock solutions were prepared by dissolving the drug in ethanol. To obtain the different drug-to-polymer ratios, the necessary quantity of stock solutions was transferred to separate tall vials. The remaining phases were carried out in the same fashion.

3. Methods

3.1 Dynamic Light Scattering (DLS)

3.1.1 Introduction

Dynamic light scattering often referred to as photon correlation spectroscopy is a method for assessing the size of colloidal dispersions that employs a monochromatic beam/source of light to illuminate a dispersion of nanoparticles or molecules experiencing Brownian motion. Brownian motion is caused by random collisions between solvent molecules and dispersed particles. The Brownian motion will therefore be slower as the particle size increases. The diffusion coefficient (D), which is correlated to the hydrodynamic size of the nanoparticle, can be determined by examining the intensity fluctuations of scattered light produced by the Brownian motion of nanoparticles in solution. It's vital to have a thorough understanding of the significance temperature poses due to the interrelation of the temperature and viscosity of a liquid. In addition, one must not forget convection currents as the temperature must be constant otherwise random motions would skew the interpretation of size. An autocorrelator, which determines the autocorrelation function of the signal, is employed in order to examine the variations in scattered light intensity.

Based on the diffusion of the particles being detected, the correlation of the signal, G, decays at an exponential rate:

$$G = B + Ae^{-2q^2}D$$

in which A represents the correlation function's baseline and B indicates its intercept. D as previously stated is the translational diffusion coefficient. The scattering vector (q) is determined by the following equation

$$q = \frac{4\pi n}{\lambda_\circ} sin\left(\frac{\theta}{2}\right)$$

in which n indicates the refractive index of the sample, λ_o is the wavelength of the laser and θ equates to the angle in which the sample is placed relative to the detector.

The practical information, which is the hydrodynamic radius (R_h), is the radius of a hypothetical sphere that diffuses at the same rate as the particle under study. The Stokes-Einstein equation can be utilized to calculate the hydrodynamic radius

$$D = \frac{kT}{6\pi\eta R_h}$$

in which k is the Boltzmann constant, T is the absolute temperature and η is the solvent's viscosity. The hydrodynamic radius is computed from the autocorrelation function after it has been processed by a mathematical algorithm. The cumulant analysis method and the normalizing techniques provided by the CONTIN software are two such algorithms that are nearly solely employed for the aforementioned analysis. According to the cumulant analysis method, the autocorrelation function is described by a polynomial, usually of the 2nd or 3rd degree, and from the coefficients of the polynomial, the diffusion coefficient (1st cumulant) and the polydispersion of the system (2nd cumulant) are obtained. The CONTIN program analyzes the autocorrelation function, which produces a huge variety of possible solutions. The more complex solutions are then eliminated because they are less likely to occur in actual systems. Of course, the final solution is not unique, thus all of the possibilities offered by the software should be considered. The size distribution function of the particles in the solution is determined by analysis using the CONTIN software.[23,67–69]

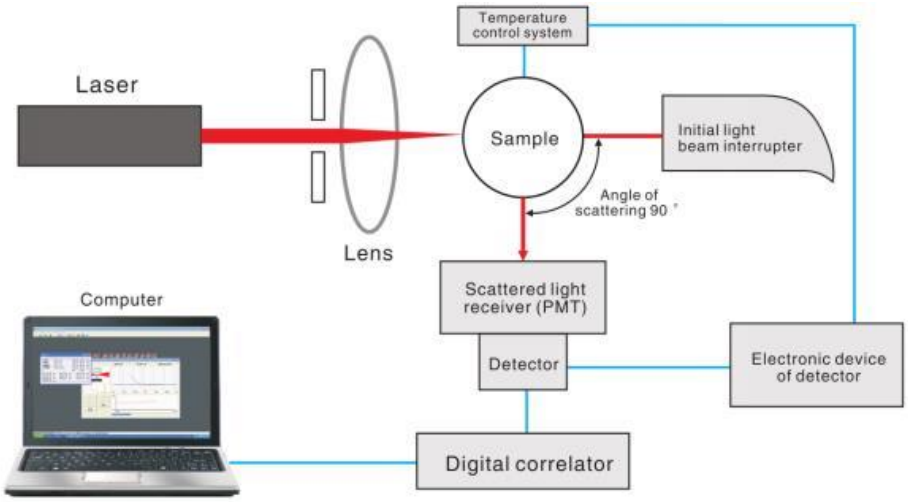

Figure 10. A schematic representation of the light-scattering instrumentation.[70]

3.1.2 Instrumentation

Dynamic light scattering measurements were performed using the ALV/CGS-3 Compact Goniometer System instrument (ALV GmbH, Germany), equipped with a JDS Uniphase 22mW He–Ne laser, operating at 632.8 nm, connected to an ALV-5000/EPP multi-tau 288-channel digital correlator (multi-time) and an electronic light scattering unit ALV/LSE-5003 to control the incremental movement of the goniometer and set the angle. The correlation functions were recorded five times and analyzed with the cumulant analysis method and the CONTIN algorithm.

3.1.3 Sample preparation

All samples were filtered with a hydrophilic syringe filter (0.45µm). Prior to use, a minuscule amount of “water for injection” was trickled through the filter to ensure the removal of dust in the filter. Before the measurement, dust in the cuvettes was removed using a rapid stream of nitrogen. After, each sample was sealed tightly with the use of parafilm and aluminum foil. The volume of each sample ranged from 0.8mL to 2mL.

3.2. Electrophoretic light scattering

3.2.1 Introduction

In an ionic solution, nanoparticles bearing a net charge will have a layer that encompasses the particle and can be separated into two sections: a layer of ions with opposite charge tightly attached to their surface, an inner region known as the Stern layer as well as an outer, a diffuse zone in which the ions are less firmly bound; hence, an electrical double layer develops over each nanoparticle. As a nanoparticle travels, for example, because of Brownian motion, a distinction is formed within the diffuse layer, ions within the barrier move with it, while ions beyond the barrier do not. This is referred to as the surface sliding plane. The electrostatic potential at this barrier is defined as the zeta potential, and it is proportional to the nanoparticle's surface charge. The peak of the zeta potential reflects the colloidal system's probable stability. In the instance, the nanoparticles have the same charge and significant value of zeta potential they will gravitate away from each other and will not agglomerate. Conversely, if the nanoparticles have low zeta potential values, they will collide and lead to sediment. To measure this value an electrical field is applied across a sample, and the charged particles dispersed in the solvent are drawn to the oppositely charged electrode. This progression is impeded by forces exerted on the nanoparticles until equilibrium. The velocity of the nanoparticles is also referred to as electrophoretic mobility. Using this data, we can use the Henry equation to calculate the particle's zeta potential.

$$U = \frac{2\varepsilon z f(\kappa\alpha)}{3\eta}$$

U stands for the velocity, ε is the dielectric constant, ζ refers to the z -potential, and f(κα) is the Henry coefficient. Two values are commonly used as estimates to determine the Henry coefficient, 1.5 or 1.0, and η is the viscosity.[71,72]

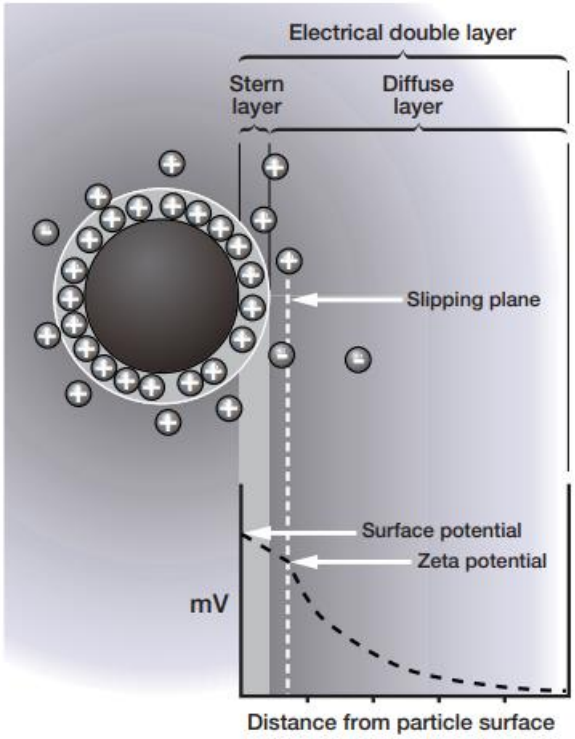

Figure 11. Schematic representation of zeta potential (ζ).[72]

3.2.2 Instrumentation

The z-potential was measured employing a Malvern system (Nano Zeta Sizer) with a 4mW He-Ne laser set at a wavelength of 633nm. It utilizes a photodiode as a detector and captures scattered radiation at an angle of 173˚ degrees. The electrokinetic measurements were performed using the LDV (Laser Doppler Velocimetry) technique using the Smoluchowski approximation, f(Ka) in this case is 1.5, to calculate the velocity and later the zeta potential values of the colloids. On average, a total of 100 measurements were obtained.

3.2.3 Sample preparation

Before usage, the dip cell must be thoroughly rinsed with distilled water and dried with a paper towel. Zeta cells should be dried with nitrogen and, if possible, opting in with new cells is highly advised. Approximately 0.3 mL of each sample was used for each measurement and discarded after.

3.3 Ultraviolet-visible spectroscopy

3.3.1 Introduction

Ultraviolet-visible (UV-vis) spectroscopy is a timely and simple characterization method commonly used in the research of nanoparticles. A good example of absorption spectroscopy is ultraviolet-visible spectroscopy, where the amount of ultraviolet or visible light wavelengths that are absorbed by or transmitted through a sample, is compared to a reference or blank sample. The excitation of electrons from a lower to higher energy state happens as a result of the UV-visible radiation being absorbed. The UV-Vis band of energy in the electromagnetic spectrum ranges from 1.5 to 6.2 eV, corresponding to a wavelength range of 800 to 200 nm. UV-Vis spectra depict the absorption A (absorbance) or transmittance T (transmittance) of incident radiation from a substance as a function of wavelength. In brief, a predetermined wavelength and intensities are aimed toward a sample, and its ultimate intensity after passing through is recorded by a detector. The light absorbed by the sample at that specific wavelength can be simply determined by comparing the incident radiation (I_0) and the transmitted radiation (I). The transmittance is calculated by the following equation:

$$T = \frac{I}{I_\circ}$$

Absorbance is the flip side of transmittance:

$$A = \log\frac{1}{T}$$

The absorbance has the potential to determine concentrations of known substances by employing the Beer-Lambert law:

$$A = \varepsilon bc$$

The units of absorbance are arbitrary units or unitless, ε is a molar absorptivity of the substance in suspension ($mol^{-1}\,L\,cm^{-1}$), b is the path length of the cuvette it typically spans 1 cm, and c is the concentration ($mol\,L^{-1}$).

There are three kinds of instrumentation one may come to find in a laboratory setting. The UV-Vis spectra can be captured through a single-beam spectrometer, double-beam spectrometer, or a simultaneous spectrometer. Under all circumstances, this equipment features a light source, a specimen holder, a wavelength selector, and a detector. The key difference between the first two comes to be the placement of a splitter and two slots for a reference sample and a specimen. To expand on this, a double-beam instrument comprises a single source as well as a monochromator, rather than a filter, accompanied by a splitter and a sequence of mirrors to direct the beam to both targets. These attributes enable more precise readings. The simultaneous instrument, on the other hand, is not equipped with a monochromator but rather features a diode array detector to simultaneously detect absorbance at all wavelengths. This option is the quickest alternative.

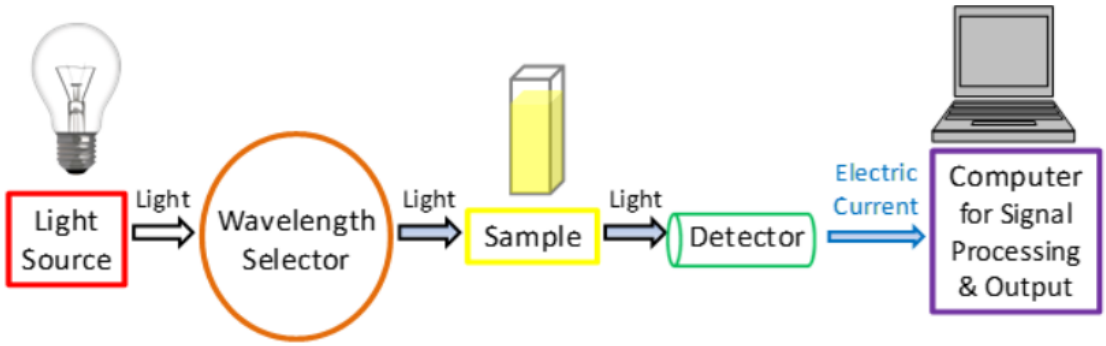

Figure 12. Illustration of the basic components of a UV-Vis Spectrometer [73]

It is important to investigate the primary elements of a UV-Vis spectrophotometer to better comprehend how it functions.

Light source:

It is commonplace to employ a single xenon lamp as a light source for both UV and visible wavelengths. Nonetheless, xenon lamps tend to be costly and less robust in the long run than two lamp systems equipped with tungsten or halogen lamps. In this configuration, a deuterium lamp is usually utilized for UV light and a tungsten or halogen lamp is frequently used for visible light. The instrument's light source must therefore swap during a measurement since two distinct light sources are required to scan both the UV and visible wavelengths. Because both light sources produce light at a comparable wavelength

between 300 and 350 nm, this swap usually takes place during this phase, allowing for a more seamless transition.

Wavelength selector:

Monochromators comprise the most widely used wavelength selectors. This device's function is to divide light into a small range of wavelengths. To select the intended wavelength of light is based essentially on using diffraction gratings that may be adjusted to select inbound and mirrored angles or by dispersion prisms. Due to the fact that the prism's material has varied refractive indices for various wavelengths of light, a prism disperses light. Despite the fact that monochromators are a common choice, filters are quite often used in conjunction with monochromators to further reduce the wavelengths of light selected and lead to better measurements and improve sensitivity.

Cuvette:

A standard cuvette can contain 3 mL of sample. Intending to avoid inaccuracies in the resultant absorption spectra, the material of the cuvettes must be chosen wisely so it does not absorb the incident light. Quartz cuvettes are primarily used.

Detector:

Using a detector, the light traveling through the specimen is converted into a usable electronic signal. Photoelectric coatings or semiconductors are extensively used in detectors. Once subjected to light, a photoelectric coating emits negatively charged electrons, and a current flow equivalent to the intensity of the light is produced. A photomultiplier tube follows this premise and is among the most prominent detectors. Similarly, an electric current corresponding to the light intensity can flow through semiconductors.[73–75]

3.3.2 Instrumentation

A Perkin-Elmer (Lambda 19) UV-Vis-NIR spectrophotometer was used to capture UV-Vis-NIR spectra. It is a double-beam spectrometer. In Figure 13 a rough depiction of this instrument can be found.

3.3.3 Sample preparation

Two Quartz cells were used, one for reference and one for each sample. For each sample 3 mL was set aside to be measured. As a sample reference, PBS was utilized.

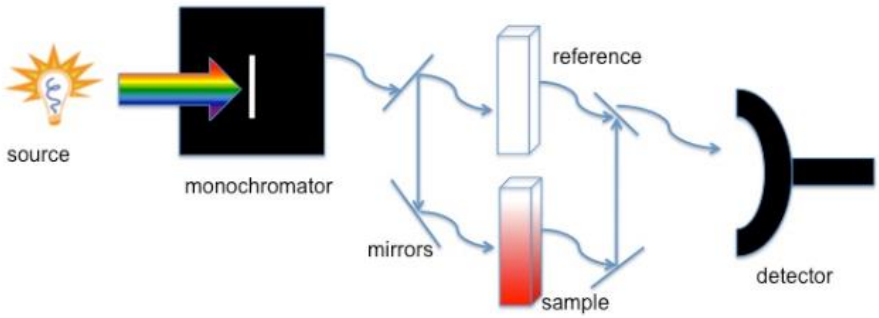

Figure 13. Schematic representation of a double beam spectrometer.[75]

3.4 Fourier transform infrared spectroscopy (FTIR)

3.4.1 Introduction

In a similar manner to UV-Vis spectroscopy, Fourier transform infrared spectroscopy (FTIR) is based on light sent through a specimen, and the intensity of the transmitted light is analyzed. Shifting from the ultraviolet and visible wavelengths of the electromagnetic spectrum to infrared enables the observation of molecular vibrational states, which reveals crucial data on aspects such as the architecture of said molecule. A molecule must have a state of vibration that produces a net change in dipole moment to absorb energy in the infrared energy spectrum. Permanent dipoles, which happen when two atoms in a molecule have considerably differing electron densities such as HCl, induced dipoles that come about with asymmetrical stretching or bending in a molecule can both generate a dipole moment. A dipole moment generates a field that interacts with radiation's electric field. The atoms that make up a compound's dipole moments will have an impact on the amount of energy needed to stretch or vibrate these bonds, which makes it possible to correlate IR absorption peaks with functional groups.

The majority of the infrared spectra from an FTIR spectrometer, which spans from 4000 to 600 cm^{-1}, are found in the mid-IR domain. Considering transition energies for a myriad of functional groups related to shifts to a vibrational excited state can be found in this domain it becomes not quite straightforward to identify whether specific functional groups are present in the structure. An FT-IR graph can be divided into four sections (Figure 14). Even though the whole FT-IR spectra has the potential to identify molecules, there is a zone which is known as the fingerprint zone. It predominately consists of multiple bands that often overlap, making this area somehow challenging to analyze, hence it is rarely utilized solely in the search for the structure, and it tends to be used only as the last step in identification.

It is important to mention peak placement is often shifted by the presence of other functional groups on the same analyte. Also, the greater the peak, the stronger the dipole moment change. In addition, stretching vibrations have often higher frequencies and demand greater energy than bending modes because it is simpler to bend molecular bonds than to stretch them. [76–78]

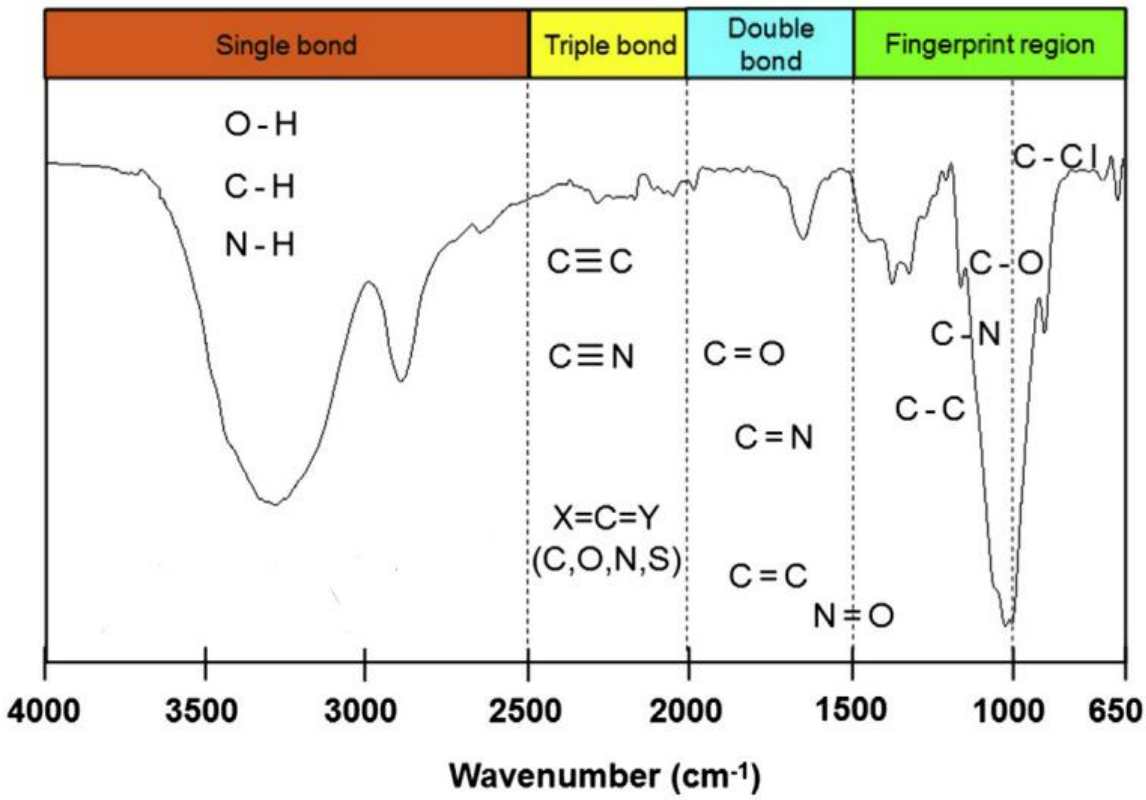

Figure 14. IR spectra domains.[78]

3.4.2 Instrumentation

An FTIR spectrometer (Bruker Optics Equinox 55) with a single reflection diamond ATR auxiliary (DuraSamp1IR II by SensIR Technologies) was utilized.

3.4.3 Sample preparation

For samples in a liquid state 80 µL were placed at the center of the diamond and dried with a stream of nitrogen. For solid samples, such as indomethacin, a tiny amount was placed on the center of the diamond.

3.5 Fluorescence spectroscopy (FS)

3.5.1 Introduction

A form of luminescence known as fluorescence occurs when molecules are struck with a certain wavelength and migrate to an exited state following the emission of a different wavelength. Fluorophores are molecules which experience these phenomena and can be observed all around us. Members of the animal kingdom, such as copepods and small reptiles, exhibit these properties for causes that are still unknown.[79]

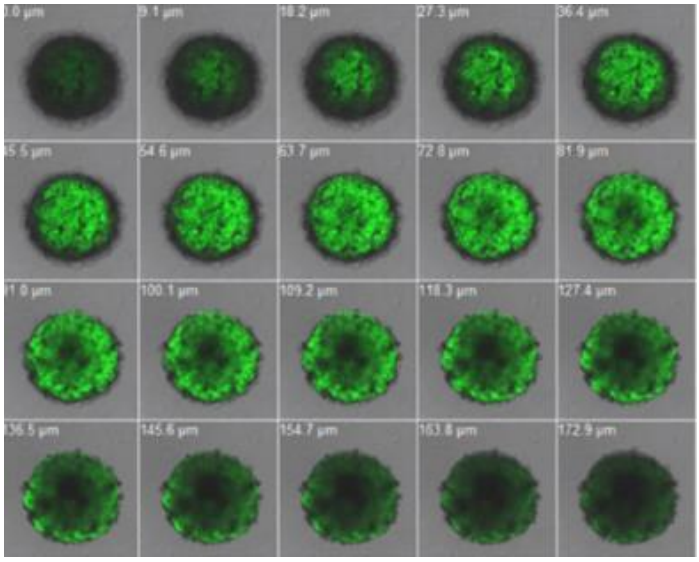

Figure 15. Curcumin-infused nanostructures used as fluorescent probe for malignant tumors. The upper-left number indicates the depth of the layer.[80]

Fluorescence spectroscopy graphs are often described as emission spectra in the scientific literature. Fluorescence spectra is a representation of the intensity of the fluorescence versus wavelength (in nanometers). The chemical structure of the fluorophore, and the solvent in which it is dispersed, both influence the emission spectra. This highly sensitive method has been utilized heavily in nanomedicine research for fluorescent drugs such as curcumin.

Fluorescence is a three-step process. The Jablonski diagram is commonly used to depict these processes. Professor Alexander Jablonski, who is considered the founder of fluorescence spectroscopy due to his many contributions, is commemorated by having his name attached to these diagrams.

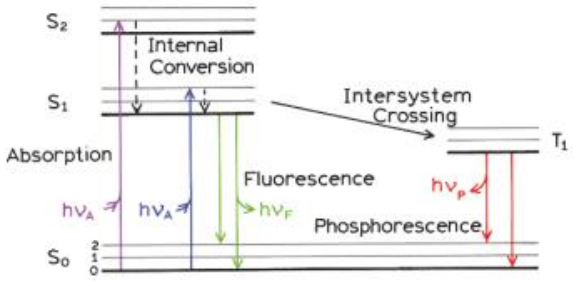

Figure 16. Jablonski diagram.[81]

Stimulation is the first stage. Most molecules at ambient temperature are within the lowest vibrational state. Thermal energy is insufficient at room temperature to occupy the excited vibrational states. The larger energy disparity between the excited states of S_0 and S_1 is just too great for thermal population of S_1. To create fluorescence, we, therefore, use light instead of heat. Essentially a fluorophore is stimulated by the absorption of ultraviolet or visible light leading to electron jumping from n non-bonding or bonding electron π orbitals to antibonding π* orbitals, causing the fluorophore to jump to a higher vibrational state S_1, S_2, and thereon. The excited state has a lifespan ranging from 1 to 10 nanoseconds. Apart from a few rare cases, known as the internal conversion phenomenon, molecules in solid or liquid states where the molecules packed close to each other tend to quickly relax to the lowest vibrational state of S_1. Although this phenomenon takes roughly 10^{-12} seconds, it's normally complete prior to emission because fluorescence lifespan is typically approaching 10^{-8} seconds. Another phenomenon that could occur is intersystem crossing. A molecule changes its spin state and is one mechanism in which it may reach a triplet excited state. The emission from this state is known as phosphorescence. This is common with heavier atoms such as iodine.

The same fluorescence emission spectrum is largely independent of excitation wavelength. This is known as Kasha's rule which is another common concept of fluorescence. Here, the surplus energy is promptly lost upon stimulation to higher states, maintaining the molecule in the lowest vibrational state of S_1. Such relaxation unfolds in a period between 10 and 12 seconds, and it is most likely the outcome of a significant amount of energy overlap among a large number of states. The key takeaways are during a transition for example S_0 to S_1, radiation proportional to the energy difference between the S_1 and S_0 states is absorbed, emission will invariably be lower in energy than absorption because of relaxation in the excited state and that emission spectra are replicas of the lowest energy absorption band due to the mirror image rule.

It is important to have a clear insight into the equipment in order to comprehend more clearly. The light source travels through a monochromator, which permits only the portion of the electromagnetic spectrum that will be employed to stimulate the molecules. Fluorescence is detected at a 90-degree angle, even though its isotropic, in an effort to

reduce the detection of the excitation beam and stray radiation. Following traveling through a single diffraction barrier emission monochromator, the emission radiation reaches the detector, which is a photomultiplier that records the radiation's intensity and delivers the information to a computer.[81–83]

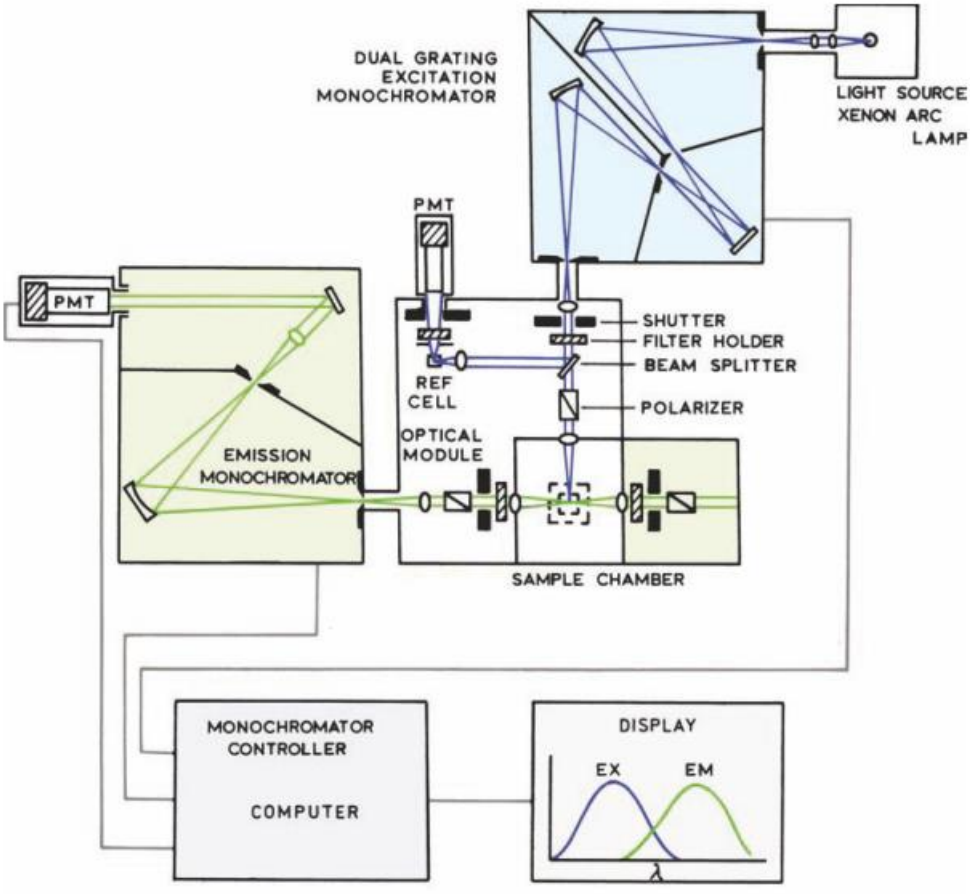

Figure 17. A spectrofluorometer. This type of instrument can measure both excitation and emission.[81]

3.5.2 Instrumentation

Fluorescence spectra were recorded on a NanoLog fluorometer (Horiba Jobin Yvon) using a laser diode as the excitation source (NanoLED, 440 nm, 100 ps pulse width) and TBX-PMT series UV detector (250-850 nm) from Horiba Jobin Yvon.

3.5.3 Sample preparation

Three milliliters were used for each measurement. The stock solution was diluted to produce various concentrations. For the pyrene assay, samples were left overnight in the dark.

Results

4.1 Self-assembly studies

4.1.1 Dynamic light scattering experiments – Protocol comparison

Dynamic light scattering experiments were conducted, in order to determine the apparent hydrodynamic radius (R_h) and the polydispersity index (PDI) of the self-assembled polymeric nanostructures. The final concentration of H-[P(OEGMA-co-LMA)] in all colloidal systems was 10^{-3} g/mL. In subsection 2.1, the preparation protocol is briefly described. Measurements were obtained at twenty-five, thirty-seven, and twenty-five degrees Celsius, to simulate conventional drug conditions and to study Pluronic's thermosensitivity. When g_H:g_{F127} is mentioned, it refers to the weight ratio of each copolymer. The Hyperbranched (H) co-polymer is H-[P(OEGMA-co-LMA)] and the triblock copolymer is Pluronic F127 (F127). Samples, after preparation, were measured the following day unless stated otherwise. The exact procedure of the sample preparation can be found in subsection 3.1.3. The goniometer was set at 90 degrees for all measurements.

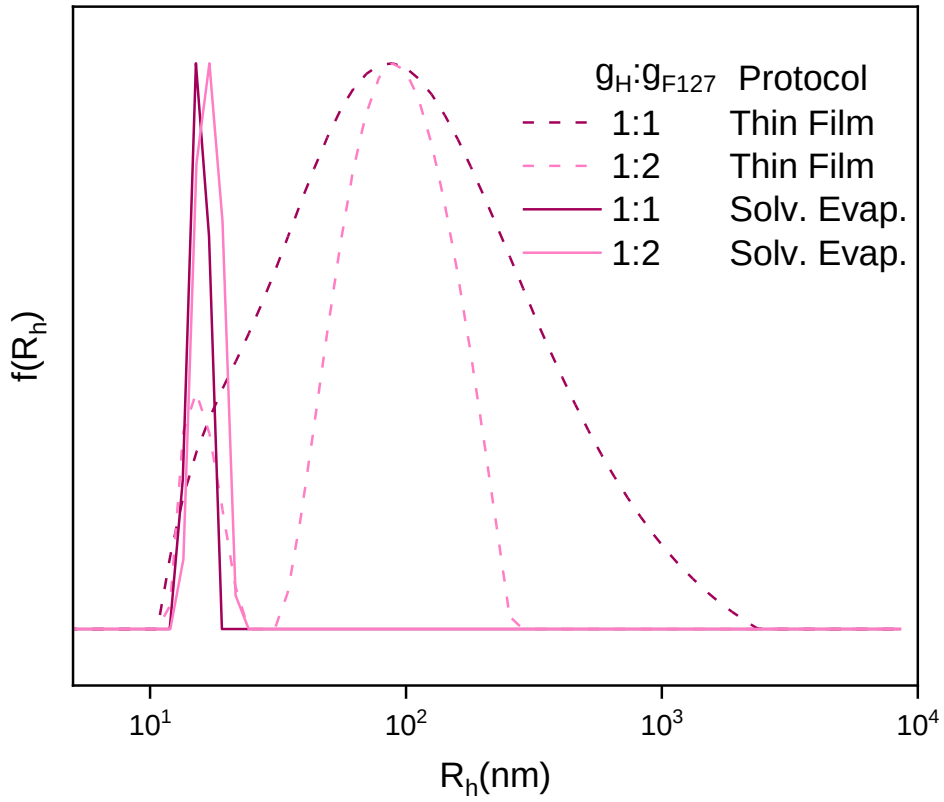

Figure 18. Protocol comparison. Size distributions from DLS analysis of the neat nanostructures H-[P(OEGMA-co-LMA)] – F127 [Thin film method (Thin film) and c-solvent evaporation protocol (Solv. Evap.), solvent: acetone→PBS]. The temperature was set at 25˚C.

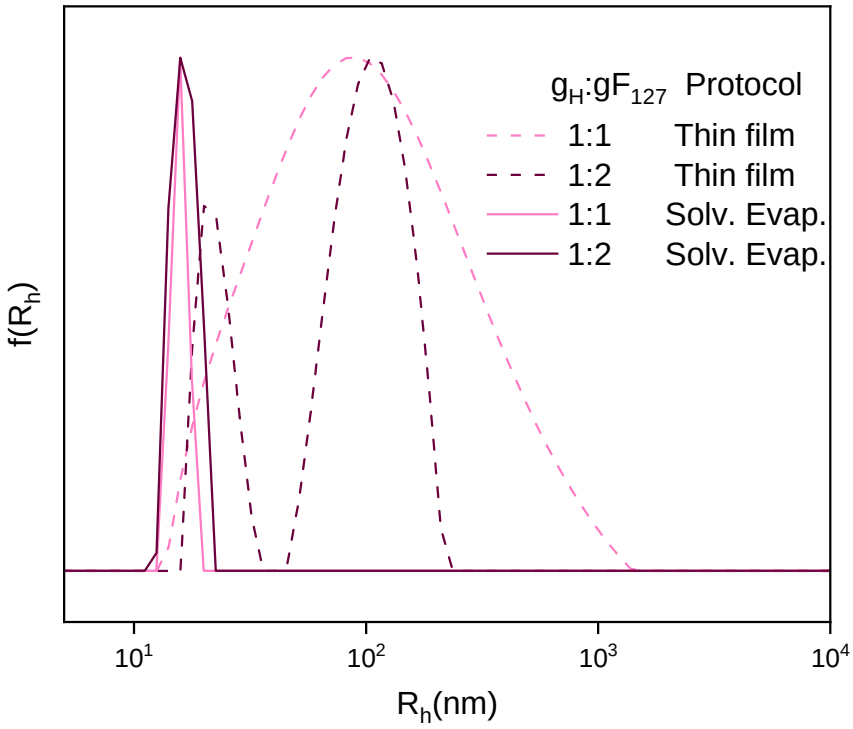

Figure 19. Protocol comparison from DLS analysis of the neat nanostructures H- [P(OEGMA-co-LMA)] – F127 [Thin film method (Thin film) and co-solvent evaporation protocol (Solv. Evap.), solvent: acetone→PBS]. The temperature was set at 37˚C.

Temperature	Intensity (A.U)	PDI	Rh(nm)	Wp(%)
H:F127 (ratio 1:1) mixed nanostructures - thin film protocol				
25˚C	950	0.492	102	>90
37˚C	316	0.439	101	>90
25˚C	300	0.496	38	>90
H:F127 (ratio 1:2) mixed nanostructures- thin film protocol				
25˚C	480	0.397	92 16	88 12
37˚C	445	0.507	104 25	75 22
25˚C	400	0.404	92 15	87 13
H:F127 (ratio 1:1) mixed nanostructures – co-solvent evaporation protocol				
25˚C	655	0.09	15	>90
37˚C	780	0.13	16	>90
25˚C	640	0.07	15	>90
H:F127 (ratio 1:2) mixed nanostructures – co-solvent evaporation protocol				
25˚C	1308	0.07	17	>90
37˚C	446	0.226	16	>90
25˚C	1297	0.06	17	>90

Table 1. Dynamic light scattering results, Protocol comparison. Acetone →PBS buffer

Based on these findings, the thin film protocol was unsuccessful in producing adequate nanostructures. Two populations are visible in both ratios, most likely due to Pluronic's thermosensitive properties. To our knowledge, the hyperbranched copolymer has not been prepared by this protocol, therefore a conclusion cannot be drawn from comparison. Based on literature review Pluronic mixed micelles (P105-F127) have been prepared in an analogous manner so the hyperbranched copolymer could play a pivotal role in the outcome.[84] On the contrary, nanostructures self-assembled from co-solvent evaporation protocol, exhibited low polydispersity indexes (PDIs) and average hydrodynamic radii (Rh) well in the range of the nanoscale varying between 15-17 nanometers. The copolymers were successfully mixed, and one population of nanostructures was recorded. H-[P(OEGMA-co-LMA)]:F127=1 mixed nanostructures prepared with the co-solvent approach produces the best outcomes out of the four exhibiting small hydrodynamic radii and low polydispersity. At body temperature, F127:H-[P(OEGMA-co-LMA)]=2 prepared with both methods revealed intriguing results that require additional investigation taking measurements at smaller increments of time. Higher percentages of the thermosensitive copolymer could likely explain the decline in intensity and increase in PDI. These aggregates begin to form smaller structures as the temperature increases making the PPO units more hydrophobic, thus explaining the increase in polydispersity.

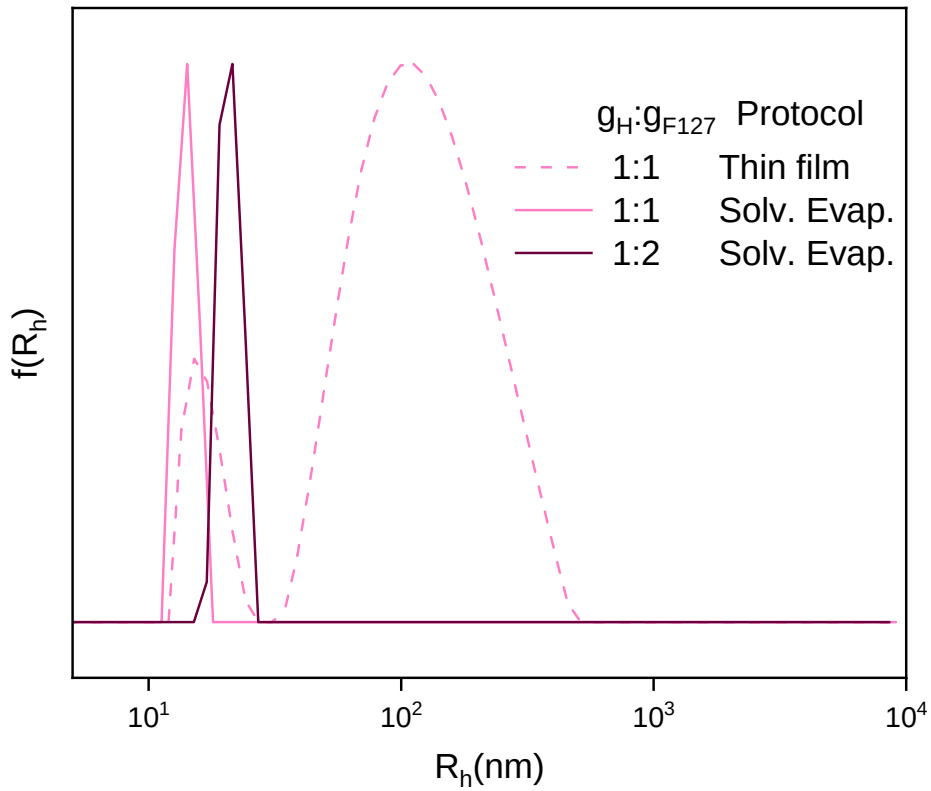

Figure 20. Protocol comparison. Size distributions from DLS analysis of the neat nanostructures H-[P(OEGMA-co-LMA)] – F127 [Thin film method (Thin film) and co-solvent evaporation protocol (Solv. Evap.), solvent: ethanol→PBS]. The temperature was set at 25˚C.

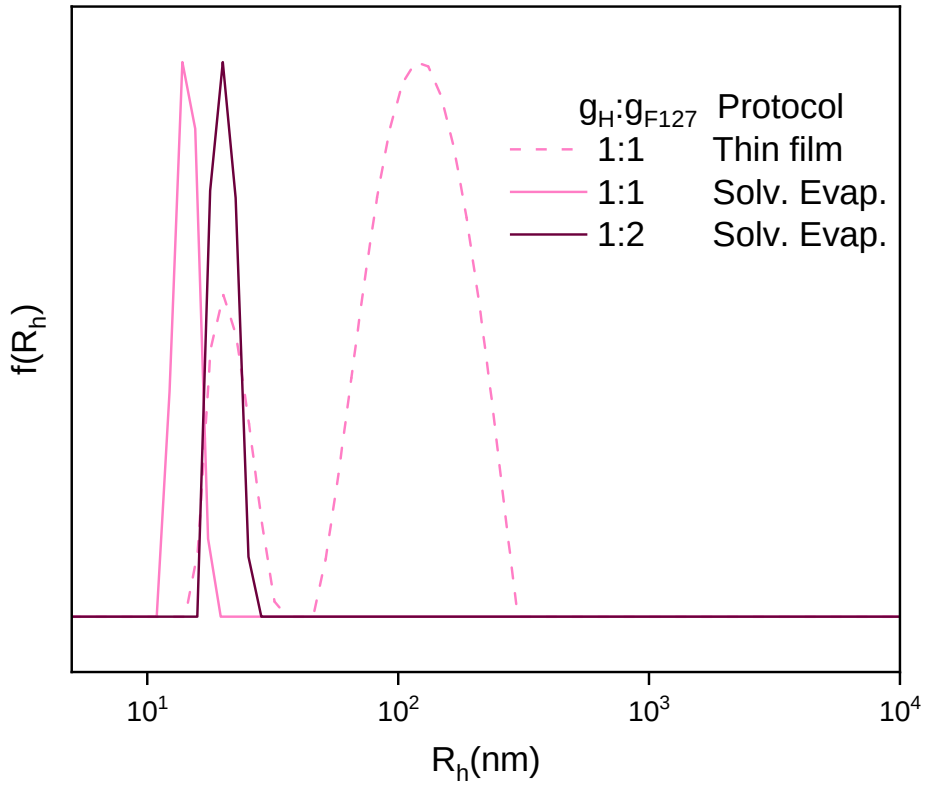

Figure 21. Protocol comparison from DLS analysis of the neat nanostructures H- [P(OEGMA-co-LMA)] – F127 [Thin film method (Thin film) and co-solvent evaporation protocol (Solv. Evap.), solvent: ethanol→PBS]. The temperature was set at 37˚C.

Temperature	Intensity(A.U.)	PDI	R_h(nm)	Wp(%)
H:F127 (ratio 1:1) mixed nanostructures - thin film protocol				
25˚C	683	0.449	119 17	88 12
37˚C	605	0.486	121 21	81 19
25˚C	568	0.4651	114	87
H:F127 (ratio 1:1) mixed nanostructures – co-solvent protocol				
25˚C	612	0.032	14	>90
37˚C	711	0.111	14	>90
25˚C	540	0.086	13	>90
H:F127 (ratio 1:2) mixed nanostructures – co-solvent protocol				
25˚C	710	0.262	21	>90
37˚C	920	0.108	20	>90
25˚C	750	0.29	20	>90

Table 2. Dynamic light scattering results, Protocol comparison. Ethanol →PBS buffer

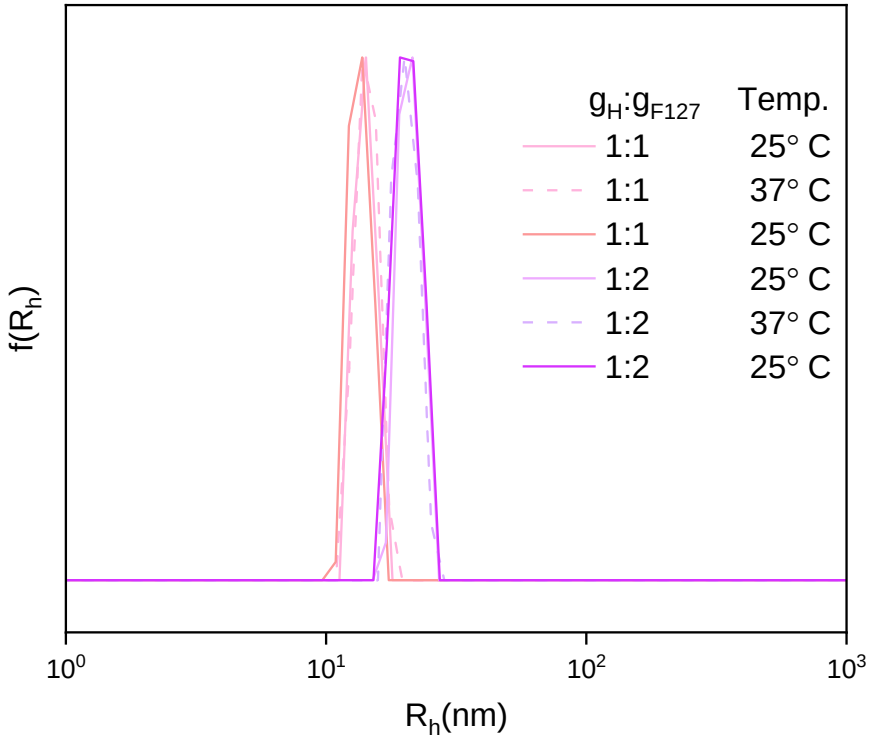

Figure 22. Ratio comparison from DLS analysis of the neat nanostructures H- [P(OEGMA-co-LMA)] – F127 [co-solvent evaporation protocol, solvent: ethanol→PBS].

It appears that the choice of solvent has no bearing on the outcome because the thin film protocol failed to form nanostructures with appropriate features, much as the acetone scenario. The use of this approach was afterward discontinued. As for the co-solvent method, the copolymers successfully combined to emerge a single type of population of nanostructures.

Small amounts of the hydrophobic copolymer exhibit less disparity and slightly smaller nanostructures, as in the case of the other solvent. As a neat nanocarrier, H-[P(OEGMA-co-LMA)]:F127=1 appears to be the most promising overall. As seen in figure 22 little to no inconsistency is exhibited throughout temperature shifts. Results were almost identical for each temperature and present desirable R_h and PDI, especially at 37˚C, which is close to body temperature. In both systems, however, there is an increase in mass at body temperature. Finally, a higher content of the triblock copolymer results in bigger structures, both in volume and mass, and this is something that is to be expected.

4.1.2 Fluorescence assay- Critical micelle concentration (CMC) / Critical aggregation concentration (CAC)

The ability of copolymers to self-assemble in aqueous media was evaluated by investigating the critical aggregation concentration (CAC). When this concentration is reached, the

formation of micelles in solutions is thermodynamically advantageous. These structures tend to disintegrate when distributed out in large volumes, like in blood circulation. The volume of blood that circulates inside a person varies according to their size, weight, and sex, but an adult human has, on average, roughly 5 liters of blood. This is problematic because micelles may abruptly leak into the bloodstream when used for drug delivery due to micelle destabilization. All of the major advantages of nanocarriers, such as increased drug load capacity, extended blood circulation, active targeting by stimuli-sensitive properties, etc., might be hampered by premature drug release, offering results comparable to those of a free drug.[85,86]

The CAC of the nanostructures was determined by fluorescence assay using pyrene as a fluorescent probe. The intensity ratio (I_1/I_3) of pyrene excitation spectra is a sensitive measure of the polarity of the microenvironment around pyrene. According to studies, as the hydrophobic component of the polymer is increased, the CMC lowers while the stability improves. An increase in the hydrophobic constituent signifies that a higher proportion of pyrene will be trapped in the aggregates. The premise of this method is that the pyrene emission spectra will be stable up until the CAC, after the fact the pyrene's fluorescence properties will subdue due to the quenching phenomenon, as pyrene is enclosed in the hydrophobic part of the aggregates.

Measurements were taken at eight different hyperbranched copolymer concentrations ranging from 10^{-3} to 10^{-8} g/mL, and the colloidal systems were obtained by being dispersed in PBS buffer. Pyrene concentration was 1mM and was dissolved in acetone. The graphs of the concentration vs intensity ratio of the relative first and third vibronic peaks I_1/I_3 are shown in the figures below. A perpendicular line is drawn at the intersection of two straight lines that are drawn in the groove of the plateau and stable points and the value of the logarithmic concentration is the critical aggregation concentration. Measurements were done on both F127:H-[P(OEGMA-co-LMA)]=2 and H-[P(OEGMA-co-LMA)]:F127=1 at ambient temperature. [42,87,88]

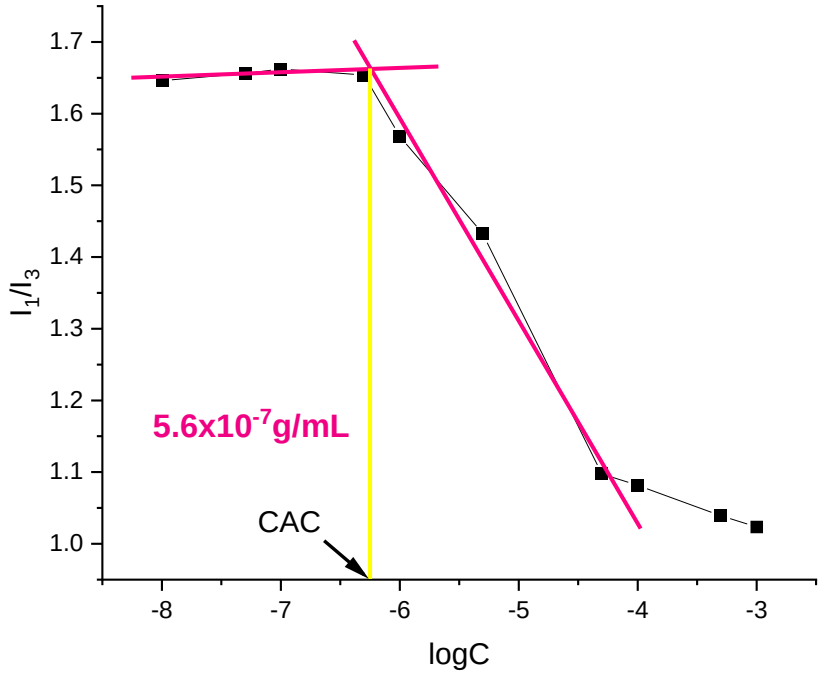

Figure 23. CAC determination of mixed nanostructures H-[P(OEGMA-co-LMA)]:F127=1, [co-solvent evaporation protocol, solvent: ethanol→PBS]

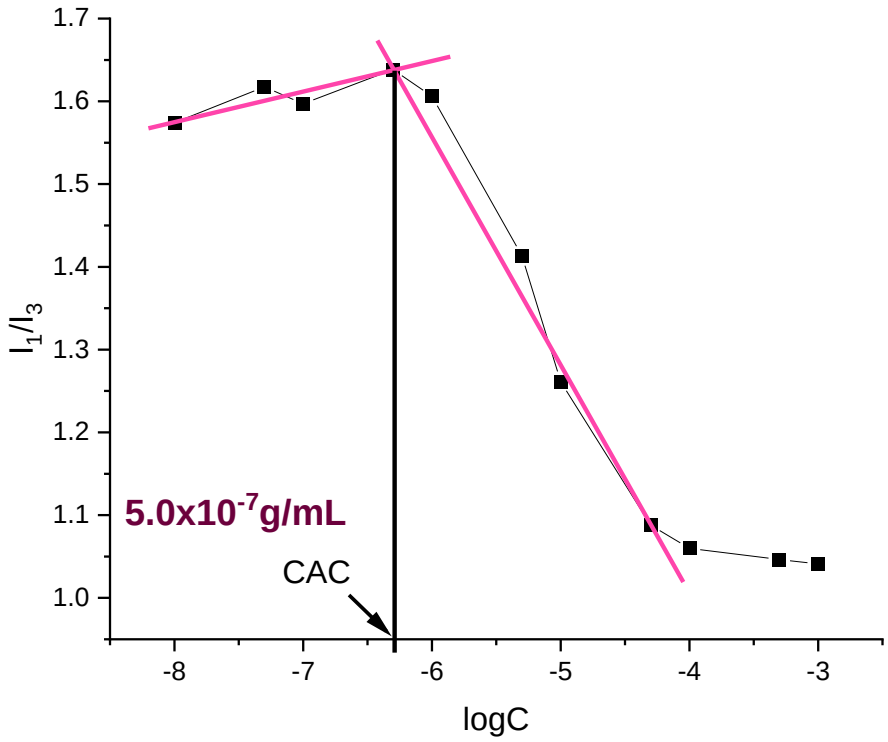

Figure 24. CAC determination of mixed nanostructures F127:H-[P(OEGMA-co-LMA)]=2, [co-solvent evaporation protocol, solvent: ethanol→PBS]

The CMC value for colloidal system H-[P(OEGMA-co-LMA)]:F127=1 was as low as $5.6x10^{-7}$ g/mL. Far yet, F127:H-[P(OEGMA-co-LMA)]=2 exhibits all the more desirable outcomes with a value of as $5.0x10^{-7}$ g/mL. Both mixed systems—Pluronic F127 ($6.9\ 10^{-5}$g/mL) [42] and H-[P(OEGMA-co-LMA) (2.5×10^{-6}g/mL) [23]—outperformed their parent copolymers, supporting the notion that mixed systems may be superior to their copolymers. A higher percentage of Pluronic copolymer seems to have favorable results with the decrease of critical micelle concentration.

4.1.3 Zeta potential determination for non-loaded/neat nanostructures

When the zeta potential of a nanoparticle is within the range of 10 and +10 mV, it is deemed to be essentially neutral, however, if it is above +30 mV or below -30 mV, it is classified as strongly cationic or anionic. Zeta potential can impact a nanoparticle's propensity to penetrate membranes as the majority of biological membranes have a negative charge. A study on both Gram-positive and Gram-negative bacteria hypothesized that positive zeta potential values may be linked to an increase in membrane permeability, and it was found that going past a certain threshold resulted in cell death due to the destabilization of the membrane. Another study on mucosal permeation revealed that negatively charged chitosan micelles had 6 times the greater capacity for mucus permeation than their positively charged counterparts.[71,72,89–91]

Dynamic light scattering (DLS) was employed to measure the zeta potential of emerged nanostructures at room temperature. Measurements for zeta potential were done in water for injection due to the high salt concentration of the buffer. Results are displayed in table 3 below.

Mixed nanostructures	Z- potential (mV)
F127:H-[P(OEGMA-co-LMA)]=1	-25.3
F127:H-[P(OEGMA-co-LMA)]=2	-18.8

Table 3. Zeta potential values for blank nanostructures

The negative z-potential values from Electrophoretic Light Scattering (ELS) measurements probably reflect the presence of carboxyl groups on the chain ends of the hyperbranched copolymer. A slightly negative surface charge may be beneficial since it does not induce interaction with serum proteins. They could be characterized as moderately unstable systems. [23]

4.2 Drug loading

4.2.1 Dynamic light scattering measurements on drug-loaded nanostructures

Taking into consideration both copolymer's biocompatibility and self-assembling behavior, the ability of the nanocarriers to encapsulate curcumin and indomethacin on separate occasions was investigated. This was done in order to obtain results on drugs with diverse levels of hydrophobicity. The colloidal systems were prepared at 10^{-3} g/mL hyperbranched copolymer concentration and the exact procedure can be found in subsection 2.1.2. The theoretical encapsulation degree of curcumin was relative to both copolymers and the two formulations of curcumin were calculated by summing up the weight ratio to 10% and 20%. Only the systems which contained 10% curcumin were able to encapsulate successfully the A.P.I. (Active Pharmaceutical Ingredient). The same scheme was followed to obtain the indomethacin-loaded nanostructures with the exception of 20% which was not investigated.

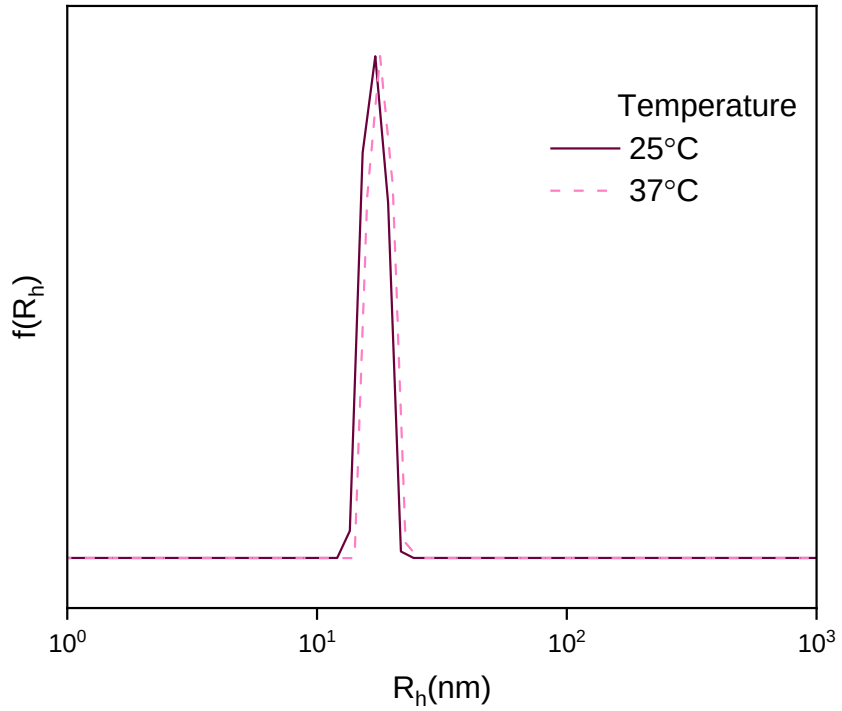

Figure 25. Temperature comparison of mixed micelles H-[P(OEGMA-co-LMA)]:F127=1 loaded with curcumin. [co-solvent evaporation protocol, solvent: ethanol→PBS] [c_H= 10^{-3} g/mL, 10% curcumin]

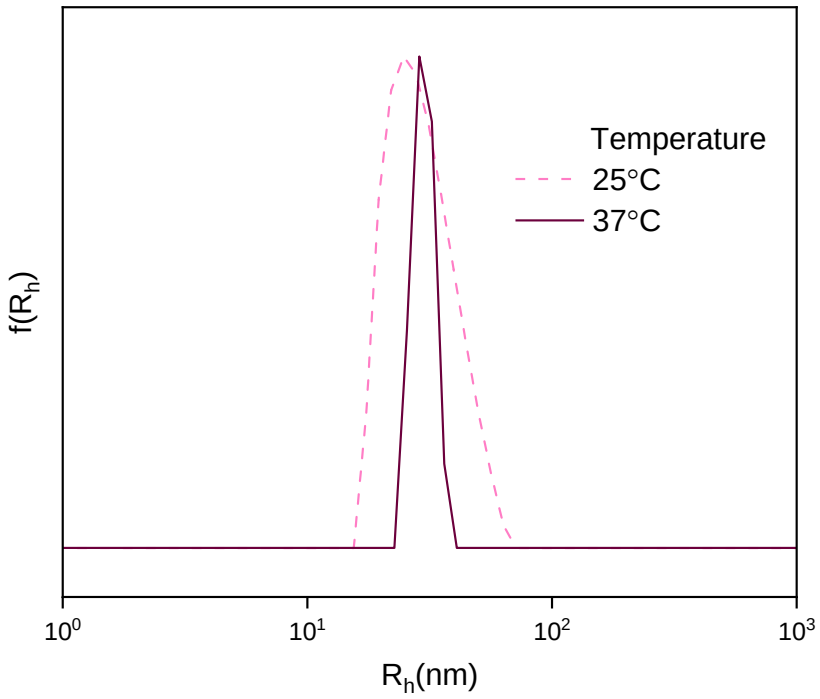

Figure 26. Temperature comparison of mixed nanostructures F127:H-[P(OEGMA-co-LMA)]=2 loaded with curcumin. [co-solvent evaporation protocol, solvent: ethanol→PBS] [c_H= 10^{-3} g/mL, 10% curcumin]

Temperature	Intensity(A.U.)	PDI	R_h(nm)	Wp(%)
H:F127 (ratio 1:1) curcumin-loaded mixed nanostructures				
25˚C	712	0.14	17	>90
37˚C	802	0.01	18	>90
H:F127 (ratio 1:2) curcumin-loaded mixed nanostructures				
25˚C	480	0.19	29	>90
37˚C	497	0.27	29	>90

Table 4. Dynamic light scattering results of mixed nanostructures loaded with curcumin. [co-solvent evaporation protocol, solvent: ethanol→PBS] [c_H= 10^{-3} g/mL, 10% curcumin]

The drug was successfully encapsulated by both H-[P(OEGMA-co-LMA)]:F127=1 and F127:H-[P(OEGMA-co-LMA)]=2 and obtained aqueous solubility. It is important to note that each had excellent results, particularly in terms of the monodispersity of the emerging structures. This is most likely due to the hydrophobic drug being tightly packed in the micelles, therefore enhancing the hydrophobic interactions. According to past research on the encapsulation of hydrophobic drugs in Pluronic copolymer micelles, the inclusion of these drugs increases the radii of the micelles. This could be because by increasing the hydrophobicity in an aqueous solution of an amphiphilic copolymer that has now formed

mixed micelles by adding a lot of more hydrophobic substances, like curcumin, typically results in an increase in the hydrodynamic radii as well because the core of the micelle becomes more strongly hydrophobic, necessitating the incorporation of more hydrophilic chains to form the hydrophilic corona protection around it making the end structure much larger. Also, even after the introduction of the drug, the structures do not surpass 50 nm in radius. For tumors with low permeability, such as pancreatic and stomach cancer, nanocarriers of this size are needed [23,36,71,92]. Similar to the neat nanostructures, F127: H-[P(OEGMA-co-LMA)]=1 performed marginally better. F127:H-[P(OEGMA-co-LMA)]=2 curcumin-loaded nanostructures seem to have a smaller mass than its's neat nanostructures. In the case of curcumin-loaded mixed nanostructures F127: H-[P(OEGMA-co-LMA)]=1, the increase in temperature, lead to less diversity and an increase in mass in the emerged nanostructures which could be explained by the increase in hydrophobicity.

Figure 27 depicts the emerged samples; each sample had a different hue of orange. The higher amount of drug was unsuccessful in producing drug-loaded micelles, the most probable scenario being that the core did not have the capacity to withstand this amount of drug.

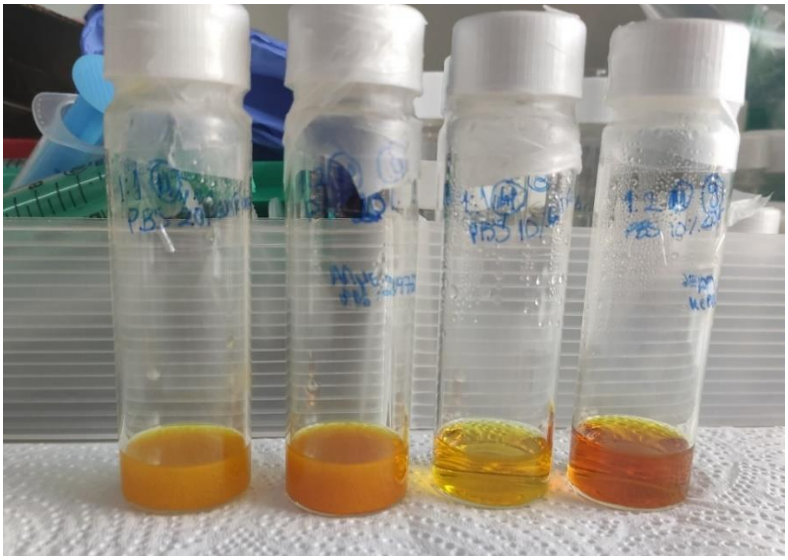

Figure 27. Emerged samples of drug loading schemes. From left to right, H-[P(OEGMA-co-LMA)]:F127=1 injected with 20%wt of curcumin, F127:H-[P(OEGMA-co-LMA)]=2 injected with 20%wt of curcumin, H-[P(OEGMA-co-LMA)]:F127=1 injected with 10%wt of curcumin, F127:H-[P(OEGMA-co-LMA)]=2 injected with 10%wt of curcumin. The higher amount of drug was unsuccessful in producing drug-loaded nanostructures.

Indomethacin was selected so that several drugs with varying levels of solubility could be assessed. Despite the fact that only one concentration of the drug was attempted, the same protocols were used for the encapsulation of indomethacin.

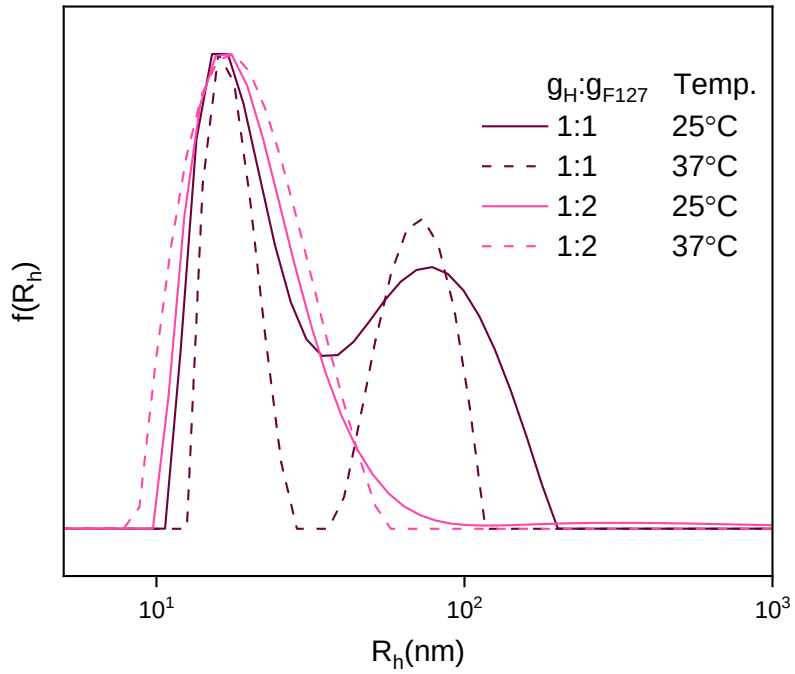

Figure 28. Ratio comparison of the indomethacin loaded mixed polymeric nanostructures H-[P(OEGMA-co-LMA)] – F127 [co-solvent evaporation protocol, solvent: ethanol→PBS]. [10% indomethacin].

Temperature	Intensity(A.U.)	PDI	R_h(nm)	Wp(%)
H:F127 (ratio 1:1) indomethacin-loaded mixed nanostructures				
25°C	431	0.351	18 75	49 48
37°C	447	0.333	69 18	49 50
H:F127 (ratio 1:2) indomethacin-loaded mixed nanostructures				
25°C	490	0.2	22	>90
37°C	575	0.182	19	>90

Table 5. Dynamic light scattering results of indomethacin-loaded mixed polymeric nanostructures H- [P(OEGMA-co-LMA)] – F127 [co-solvent evaporation protocol, solvent: ethanol→PBS]. [10% indomethacin].

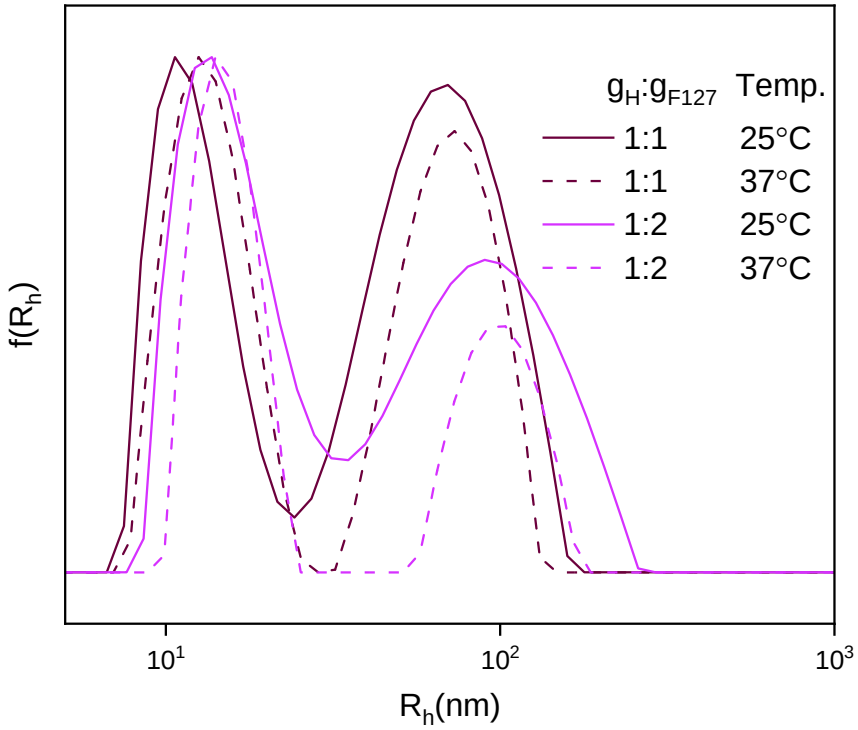

Figure 29. Ratio comparison of indomethacin loaded mixed polymeric nanostructures H-[P(OEGMA-co-LMA)] – F127 [co-solvent evaporation protocol, solvent: ethanol→WFI]. [10% indomethacin]

Temperature	Intensity(A.U.)	PDI	R_h(nm)	Wp(%)
H:F127 (ratio 1:1) indomethacin-loaded mixed nanostructures				
25˚C	669	0.441	34	>90
37˚C	726	0.419	13 70	48 50
H:F127 (ratio 1:2) indomethacin-loaded mixed nanostructures				
25˚C	793	0.432	36	>90
37˚C	874	0.39	98 15	37 61

Table 6. Dynamic light scattering results of indomethacin loaded mixed polymeric nanostructures H- [P(OEGMA-co-LMA)] – F127 [co-solvent evaporation protocol, solvent: ethanol→WFI]. [10% indomethacin]

Due to unforeseen circumstances, measurements on the samples prepared with water for injection took place 10 days later instead of 1 day after preparation. In almost all samples

two distinct populations were recorded. In a similar manner with indomethacin-loaded Pluronic micelles, there is a decrease in the observed radii with the introduction of the hydrophobic drug.[31] F127:H-[P(OEGMA-co-LMA)]=2 prepared with PBS yielded structures with favorable properties. It exhibited low polydispersity indexes (PDIs) and average hydrodynamic radii (Rh) well in the range of the nanoscale varying between 19-21 nanometers depending on the temperature. When compared with the mixed nanostructures F127:H-[P(OEGMA-co-LMA)]=2 loaded with curcumin, although having comparable PDIs, they are smaller in size. For reference, Pluronic F127 and other poloxamers commonly generate bigger micelles sizes ranging from 20 to 50nm when introduced to curcumin to compensate the hydrophobicity.[93,94] Also, the suspension agent seems to have an effect on the size and PDI of the emerged structures recording different results with PBS and WFI. As for the rest of the samples, conclusions should not be made quite yet as stability studies appear to put things in perspective.

4.2.2 Zeta potential determination for loaded nanostructures

Dynamic light scattering (DLS) was employed to measure the zeta potential of emerged micelles at room temperature. Due to the buffer's high salt content, zeta potential measurements were performed on colloidal systems prepared in water for injection. We anticipate that the colloidal systems dispersed in PBS will produce different zeta potential results due to the fact that the DLS data also defers from water to PBS for indomethacin loaded mixed polymeric nanostructures H- [P(OEGMA-co-LMA)] – F127. Results for drug-loaded mixed nanostructures are displayed in Table 7 below.

Mixed nanostructures	Z- potential (mV)
F127: H-[P(OEGMA-co-LMA)]=1 10% curcumin	-15.2
F127:H-[P(OEGMA-co-LMA)]=2 10% curcumin	-2
F127:H-[P(OEGMA-co-LMA)]=1 10% indomethacin	-22.7
F127:H-[P(OEGMA-co-LMA)]=2 10% indomethacin	-19

Table 7. Zeta potential values for drug-loaded nanostructures.

The majority of the samples appear to be colloidally unstable. The F127:H-[P(OEGMA-co-LMA)]=2 (10% curcumin) zeta potential value of -2mV ought to be relatively close to the rest of the samples due to the high standard deviation. The carboxyl group is most likely the source of the negative charge, as was stated in the preceding chapter. The aggregates of the drug-loaded hyperbranched copolymer yield similar findings. Although there is a modest drop in comparison to the neat nanostructures, it is most likely due to the introduction of the A.P.I. as it acts as a compensating factor.

It is important to note that, while colloidal stability is associated with greater z potential values, the reality is more nuanced. Zeta potential serves as an indicator, but it does not provide the complete picture. As stated in the literature review section, colloid stability is determined by the sum of van der Waals attractive forces and electrostatic interactions and because of this, stable colloidal suspensions with moderate zeta potential and vice versa are not rare. Additionally, we must take into account PEGylation, which is known to increase nanoparticle durability while lowering zeta potential by masking negatively charged nanoparticles.[23,89,95]

Every sample exhibited a negative zeta value, which is essential for in vitro applications. Compared to neutral or anionic particles, cationic particles are more cytotoxic and more prone to cause hemolysis and blood clotting. Also, positively charged nanoparticles tend to quickly gravitate toward the liver, spleen, and lungs while neutral or slightly negatively charged nanomedicines circulate for a longer period of time in the bloodstream.[36,96]

4.3 Stability studies

4.3.1 Stability studies – Neat nanostructures

Dynamic light scattering measurements were used to inspect the samples temporal stability. To prevent batch-to-batch variability, the same stock solution was utilized (with the exception of the dialysis assay), and it was kept airtight to prevent contamination. Samples were measured at different timeframes, each of which is stated on the DLS graphs.

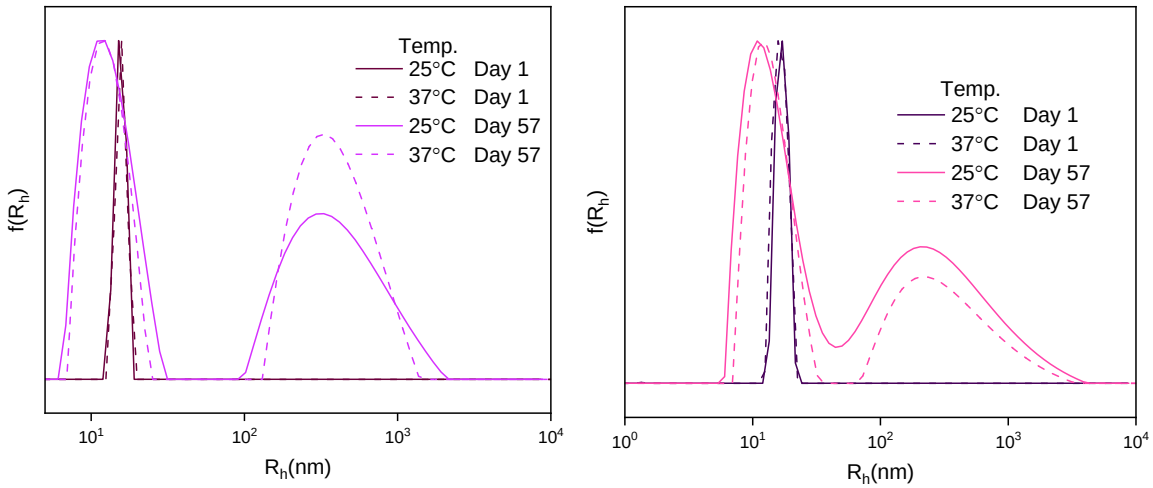

Figure 30. Stability studies from DLS analysis of the unloaded mixed polymeric nanostructures H-[P(OEGMA-co-LMA)]:F127=1(left) and F127:H-[P(OEGMA-co-LMA)]=2(right) [co-solvent evaporation protocol, solvent: acetone]

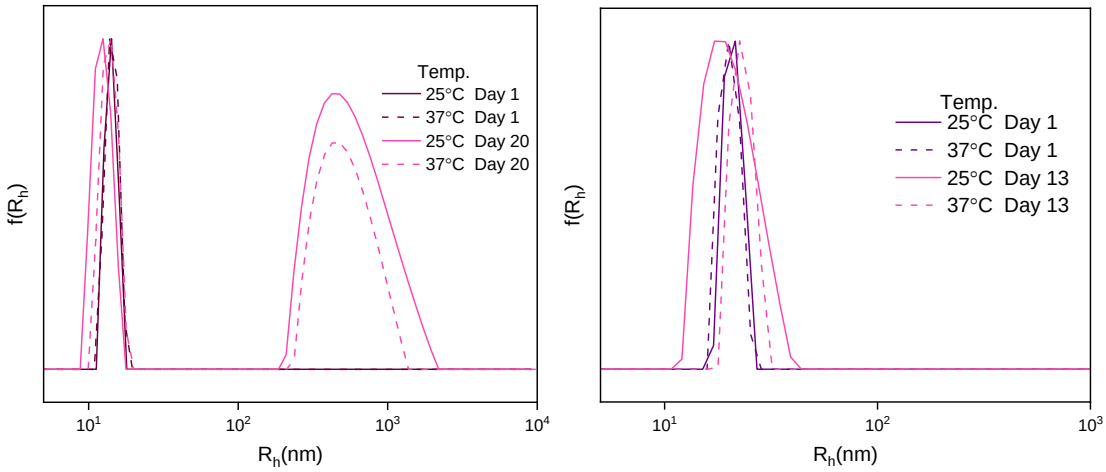

Figure 31. Stability studies from DLS analysis of the unloaded mixed polymeric nanostructures H-[P(OEGMA-co-LMA)]:F127=1(left) and F127:H-[P(OEGMA-co-LMA)]=2 (right) [co-solvent evaporation protocol, solvent: ethanol]

Timeframe	Temperature	Intensity(A.U.)	PDI	R_h(nm)	Wp(%)
H:F127 (ratio 1:1) blank mixed nanostructures-co-solvent method-acetone					
Day 1	25˚C	655	0.09	15	>90
	37˚C	780	0.13	16	>90
Day 57	25˚C	865	0.446	13 380	51 47
	37	980	0.468	12 400	45 42
H:F127 (ratio 1:2) blank mixed nanostructures-co-solvent method- acetone					
Day 1	25˚C	1308	0.07	17	>90
	37˚C	446	0.226	16	>90
Day 57	25˚C	371	0.47	55	>90
	37˚C	515	0.465	31 130	40 57
H:F127 (ratio 1:1) blank mixed nanostructures-co-solvent method-ethanol					
Day 1	25˚C	612	0.032	14	>90
	37˚C	711	0.111	14	>90
Day 20	25˚C	525	0.608	12 55 9	24 70 6
	37˚C	570	0.563	14 51	31 69
H:F127 (ratio 1:2) blank mixed nanostructures-co-solvent method-ethanol					
Day 1	25˚C	710	0.262	21	>90
	37˚C	920	0.106	20	>90
Day 13	25˚C	716	0.04	20	>90
	37˚C	906	0.02	23	>90

Table 8. Dynamic light scattering results of neat mixed polymeric nanostructures H- [P(OEGMA-co-LMA)] – F127 [co-solvent evaporation protocol]

In the absence of the hydrophobic drug, the morphology of these nanostructures can change over time. Micelles that heavily rely on hydrophobic interactions to stabilize their structure may produce more thermodynamically stable formations that lack the properties necessary for efficient nanocarriers. This is true of the emerged nanostructures, regardless of which solvent was utilized. The hydrodynamic distribution suggests that the same nanostructures have a propensity to coagulate, which appears to be the most plausible scenario. This finding may also aid in understanding the rise in PDI. For at least two weeks, F127:H-[P(OEGMA-co-LMA)]=2 (ethanol→PBS) was able to maintain its consistency with few to no variations in hydrodynamic radii. It is interesting to observe that it nearly achieved monodispersity with this settling time. It also acquires mass and volume at 37°C as in the first measurement. There was no visible sedimentation in any of the samples to suggest the structures were not in suspension.

4.3.2 Stability studies- drug-loaded nanostructures

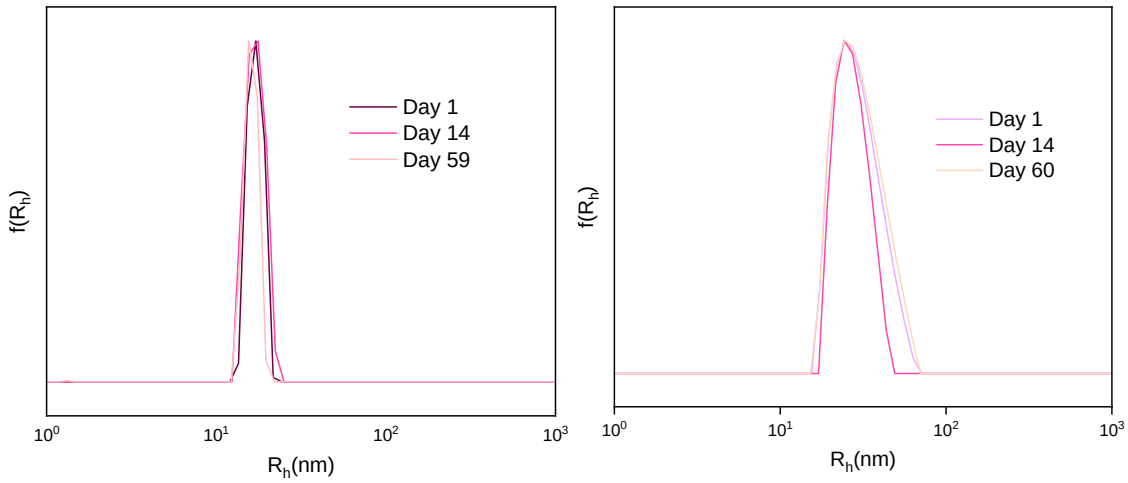

Figure 32. Stability studies from DLS analysis of the curcumin loaded mixed polymeric nanostructures H-[P(OEGMA-co-LMA)]:F127=1(left) and F127:H-[P(OEGMA-co-LMA)]=2 (right) [co-solvent evaporation protocol, solvent: ethanol→PBS]. Temperature: 25˚C.

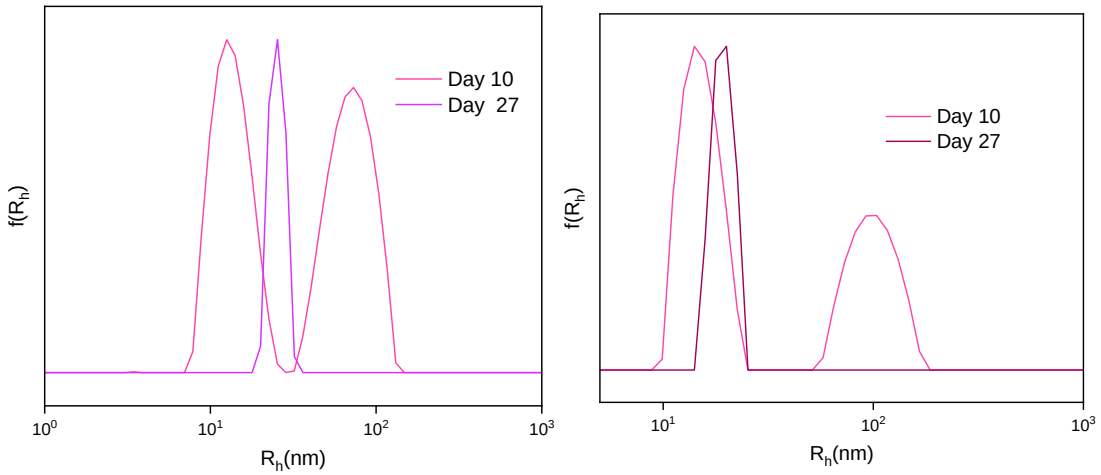

Figure 33. Stability studies from DLS analysis of the indomethacin loaded mixed polymeric nanostructures H-[P(OEGMA-co-LMA)]:F127=1(left) and F127:H-[P(OEGMA-co-LMA)]=2(right) [co-solvent evaporation protocol, solvent: ethanol→WFI]. Temperature: 37˚C.

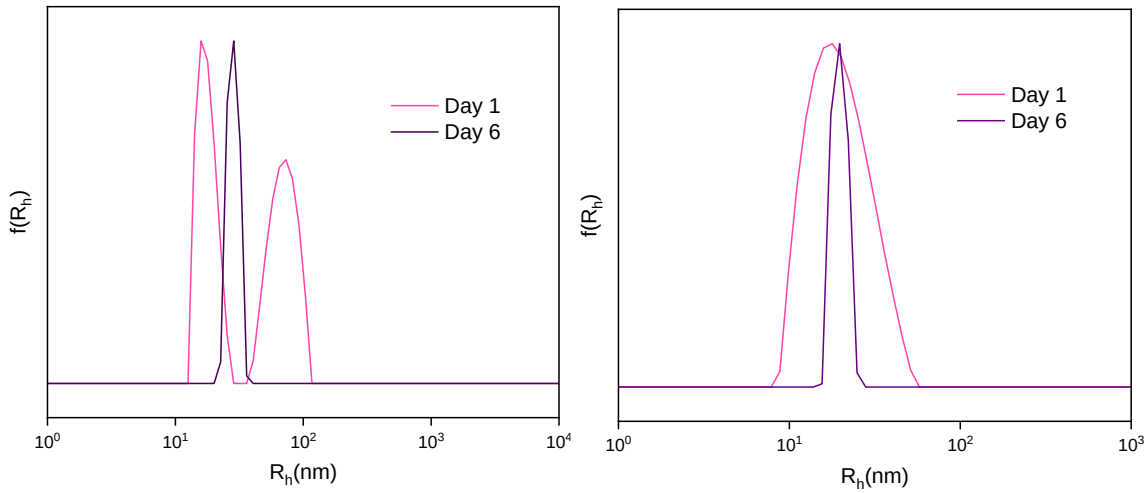

Figure 34. Stability studies from DLS analysis of indomethacin loaded mixed polymeric nanostructures H-[P(OEGMA-co-LMA)]:F127=1(left) and F127:H-[P(OEGMA-co-LMA)]=2(right) [co-solvent evaporation protocol, solvent: ethanol→PBS]. Temperature: 37˚C.

Timeframe	Temperature	Intensity(A.U.)	PDI	R_h(nm)	Wp(%)
H:F127 (ratio 1:1) curcumin-loaded mixed nanostructures-PBS					
Day 1	25˚C	712	0.14	17	>90
Day 14		624	0.078	17	>90
Day 59		653	0.123	16	>90
H:F127 (ratio 1:2) curcumin-loaded mixed nanostructures-PBS					
Day 1	25˚C	480	0.19	29	>90
Day 14		385	0.01	27	>90
Day 60		1023	0.06	29	>90
H:F127 (ratio 1:1) indomethacin-loaded mixed nanostructures-WFI					
Day 10	37˚C	726	0.419	13 70	48 50
Day 27		935	0.415	25	>90
H:F127 (ratio 1:2) indomethacin-loaded mixed nanostructures-WFI					
Day 10	37˚C	874	0.39	98 15	37 61
Day 27		1129	0.07	24	>90
H:F127 (ratio 1:1) indomethacin-loaded mixed nanostructures -PBS					
Day 1	37˚C	447	0.333	69 18	49 50
Day 6		550	0.016	31	>90
H:F127 (ratio 1:2) indomethacin-loaded mixed nanostructures-PBS					
Day 1	37˚C	575	0.182	19	>90
Day 6		741	0.02	19	>90

Table 9. Dynamic light scattering results of drug-loaded mixed polymeric nanostructures H-[P(OEGMA-co-LMA)] – F127 [co-solvent evaporation protocol].

The mixed nanostructures containing curcumin displayed adequate integrity. There were no new populations recorded. Similar studies have demonstrated that Pluronic F127 and curcumin's hydrophobic interactions have a significant impact on storage stability. The hydrophobic drug and micelle core primarily interact at the hydrophobic methyl group in the PPO chain of the Pluronic triblock copolymer. The fact that Pluronic F127 has more hydrophobic interaction sites compared to alternative poloxamers is one of the reasons it is preferred.[59,60] However, the largest structural changes were evident in the indomethacin-loaded micelles. It appears that both kinds of systems took much longer to adjust to their preferred structures. Salinity appears to have an impact on this transformation as a good amount of time was required for the nanostructures dispersed in water to come to this change. Support for this idea can be found in the fact that the second ratio of the nanostructures which were dispersed in the PBS buffer had already complied with a more advantageous structure from the start. With the exception of H-[P(OEGMA-co-LMA)]:F127=1(WFI), all indomethacin-loaded mixed systems were near to reaching a faultless PDI. The most ideal drug-loaded nanocarrier was F127:H-[P(OEGMA-co-LMA)]=2 with an Rh value of 19 nanometers and PDI 0.02. It also was able to retain its original physicochemical characteristics with the exception of its mass. In all samples, no sedimentation was visible.

4.3.3 Stability studies -Dialysis assay

Dynamic light scattering measurements for F127:H-[P(OEGMA-co-LMA)]=2 were done as part of the drug release experiment. The dialysis tubbing approach is a straightforward method to examine how drugs might distribute in circulation. In a 250 mL beaker, 100 mL of freshly prepared phosphate-buffered saline was set aside. 5 mL of stock solution was transferred to a dialysis tube. Prior to use, the dialysis tube was left to soak for 10 min. After a week of simulated circulation, the contents of the tubing were transferred to a cuvette following the DLS protocol (subsection 3.1.3). As depicted in the subsequent graph, the loaded micelles demonstrated adequate integrity following a week in the dialysis tubing that persisted over time. Batch-to-batch variability may be the cause of the different hydrodynamic radii. For future reference, DLS measurements must be performed both prior to and following dialysis. The lowest PDI value of this ratio, overall compared to all readings obtained with curcumin-loaded nanocarriers, was obtained on the 37th day, which is an intriguing indication. The dialysis procedure could be an effective strategy for drug loading for F127:H-[P(OEGMA-co-LMA)]=2.

Timeframe	Temperature	Intensity(A.U.)	PDI	R_h(nm)	Wp(%)
H:F127 (ratio 1:2) curcumin-loaded mixed nanostructures					
Stock solution	37˚C	497	0.27	29	>90
After dialysis		505	0.286	22	>90
Day 37		405	0.117	21	>90

Table 10. Dynamic light scattering results of drug-loaded mixed polymeric nanostructures F127:H-[P(OEGMA-co-LMA)]=2.

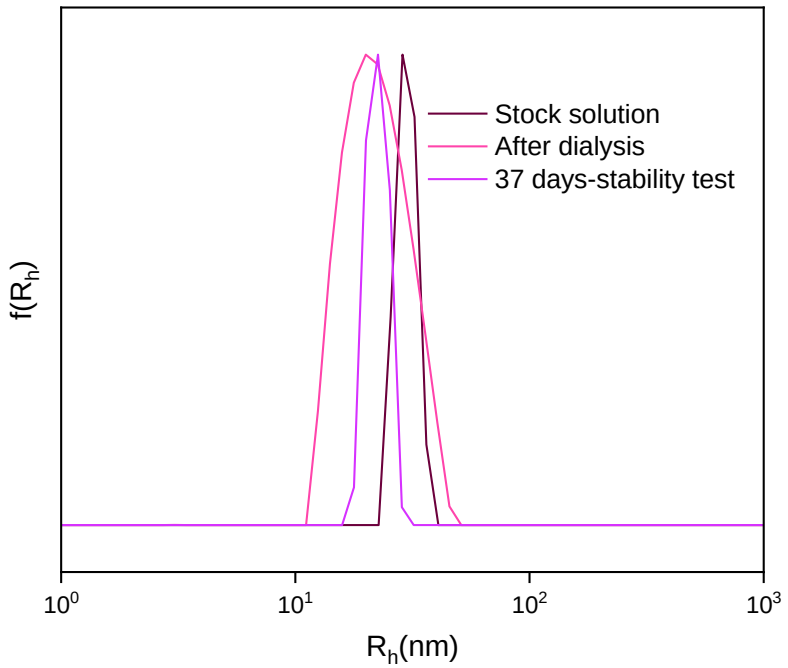

Figure 35. Stability studies from DLS analysis of curcumin-loaded mixed polymeric nanostructures F127:H-[P(OEGMA-co-LMA)]=2 [co-solvent evaporation protocol, solvent:ethanol→PBS] Temperature 37 ˚C

4.4 Bioimaging study

4.4.1 Drug release assay

The premature release of such drugs negates the use of mixed micelles as a novel probe. Therefore, a dialysis methodology was carried out to ascertain when and whether these nanocarriers would rupture and release the hydrophobic drug curcumin. The drug release assay provided by dialysis-based experiments is an easy and well-liked approach that has already been broadly utilized in pharmaceutical research in the production and quality control and as a model to establish the nanoparticle formulation's in-vitro/in-vivo correlation (IVIVC). This methodology employs dialysis tubing with a specific molecular

weight cut-off as a physical barrier. The colloidal system is situated inside the tube, which is also known as the donor compartment. It is subsequently dialyzed against an aqueous solution, in this case, phosphate buffer saline, which is referred to as the receiver compartment. The aqueous buffer should enter the hydrophilic branches and create water-filled pore structures through which the drug can diffuse. The drug subsequently diffuses through the hydrophobic core toward the donor solution before traveling through the dialysis tubing to arrive at the receiver compartment. As a consequence, the free drug release kinetics and drug permeation kinetics have an effect on the method's outcomes. Although the latter is thought to be too quick of a process to be accounted for, so the apparent drug release kinetics is commonly perceived as the true drug release kinetics.

The entire process that was followed is described in subsection 4.3.3. The samples were set in constant agitation after each measurement in which the receiver solution was supplemented with 3mL of PBS. It is a widespread practice to match the receiver solution with the dispersion agent of the suspension. Since a double-beam UV spectrometer was being used, a reference cuvette containing PBS was put aside and used as the reference for all measurements during the same day. In the figures below, both ratios' UV spectra are depicted. According to research on curcumin in comparable conditions, it does not seem to leak into the receptor solution. In the 420 nm range, there are no peaks that can be noticed.[97–102] This suggests that the free drug could not escape from the nanocarrier. Additionally, the receptor solution was never significantly tinted, even after the completion of the experiment, and only bacterial growth could be observed. Under these circumstances, when compared to the DLS data, the micelles appear to retain their structure.

For future research, a larger volume of PBS should be utilized as these results indicate that this nanocarrier could be employed as a bioimaging probe to ensure the continuous distribution of curcumin throughout the bloodstream.

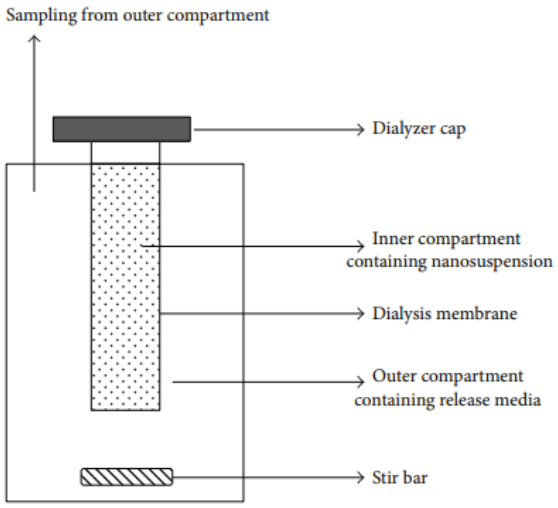

Figure 36. Schematic representation of the dialysis approach.[102]

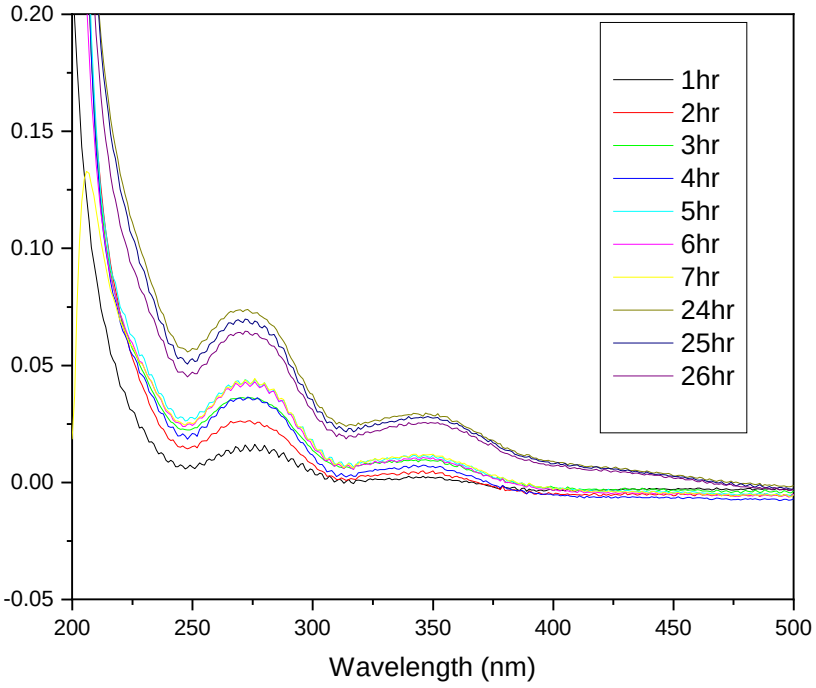

Figure 37. Drug release analysis using U.V. spectroscopy, mixed polymeric nanostructures H-[P(OEGMA-co-LMA)]:F127=1 loaded with curcumin prepared using the co-solvent evaporation approach (ethanol→PBS). [c_H= 10^{-3} g/mL, 10% curcumin] Curcumin was not recorded to be present out of the dialysis tubbing.

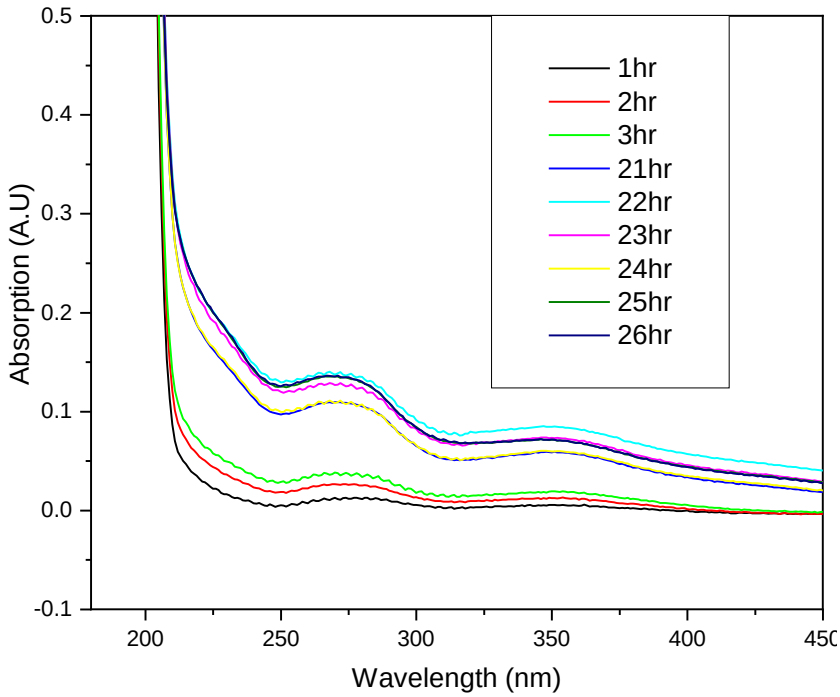

Figure 38. Drug release analysis using U.V. spectroscopy, mixed polymeric nanostructures F127:H-[P(OEGMA-co-LMA)]=2 loaded with curcumin prepared using the co-solvent evaporation approach (ethanol→PBS). [c_H= 10^{-3} g/mL, 10% curcumin] Curcumin was not recorded to be present out of the dialysis bag

4.4.2 Fluorescence assay

Curcumin has been used extensively in bioimaging research.[98] It was investigated using fluorescence spectroscopy to ascertain if the same fluorescent qualities persisted following micellization. Curcumin excitation wavelength was set at 405 nm. The concentration for H-[P(OEGMA-co-LMA)]:F127=1 was $1.0x10^{-4}$ g/mL and for F127:H-[P(OEGMA-co-LMA)]=2 was $1.5x10^{-4}$g/mL. The obtained loaded nanostructures retained curcumin's fluorescent abilities. Although the outcome defies the norm of higher concentrations producing a greater intensity. This could be explained by the notion that depending on the concentration, nanostructures alter their forms. This is a transformation described as self-quenching. The typical peak of curcumin in acetone is at 504 nm. H-[P(OEGMA-co-LMA)]:F127=1 (curcumin 10%) exhibits a slight shift to 507 nm and F127:H-[P(OEGMA-co-LMA)]=2 (curcumin 10%) a shift to 527 nm. This displacement was most likely brought on by the hydrophobic interactions between curcumin and the hydrophobic PPO and LMA units of both copolymers. All in all, the obtained loaded nanostructures retained curcumin's fluorescent abilities and attained water solubility. [103]

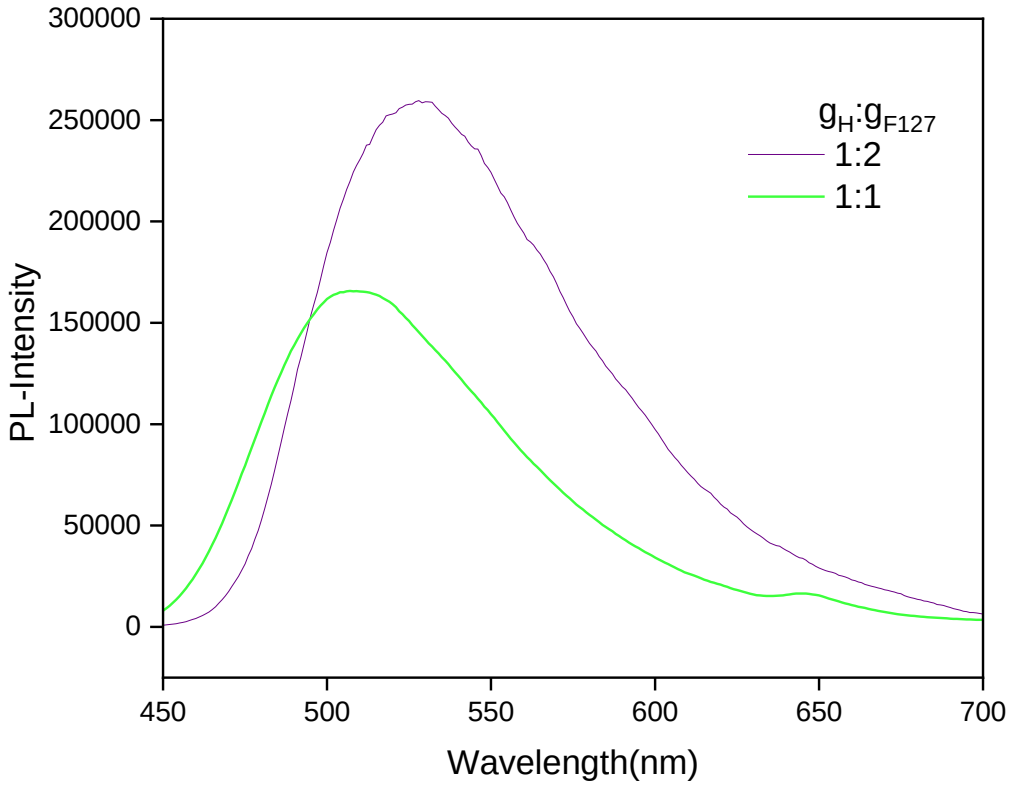

Figure 39. Ratio comparison from PL results of mixed polymeric nanostructures H-F127 loaded with curcumin dispersed in PBS. [10% curcumin].

4.5 Effect of fetal bovine serum on the integrity of the micelles

4.5.1. Dynamic light scattering measurements-FBS interactions

Fetal bovine serum is a byproduct of the meat packing industry. It is widely utilized in both academic and industry research in a multitude of applications. There are over 1,800 proteins in this type of serum, according to recent proteomic research. The primary protein is bovine serum albumin (BSA) with a concentration of about 2.5 mg/mL. Given its accessibility, FBS is widely used in nanotechnology to simulate the conditions under which a nanoparticle might come about in the bloodstream. When nanoparticles are incubated in a protein suspension, the proteins frequently adhere to the particle surface and form a protein corona that changes the surface chemistry of the nanoparticles. These phenomena could have an effect on the stability and clearance pathways of nanoparticles in vitro. It is therefore crucial to characterize the physicochemical properties of nanoparticles in such conditions.[104–108]

Eight samples in total were characterized to collect data under various scenarios. Analysis was done on curcumin-loaded mixed polymeric nanostructures H-[P(OEGMA-co LMA)]:F127=1 and F127:H-[P(OEGMA-co-LMA)]=2 that were prepared with the co-solvent protocol (ethanol→PBS). A hot plate and a water bath were employed to thaw the fetal bovine serum. The temperature was set at 37˚C. Prior to this experiment, DLS measurements were performed on the reference stock solution. The FBS suspension was then combined with each sample in either of the two different ratios in a form of volume, 1:10 or 1:1 (v/v) nanocarrier: FBS suspension. Additionally, two separate ratios—1:9 or 1:1 (v/v) FBS:PBS —of the FBS suspension were prepared. Samples were kept at 37^{o}C in a standard glassware oven to evaluate how these systems would respond over a longer period of time under these conditions.

F127:H-[P(OEGMA-co-LMA)]=2 must be credited as the mixed system that performed best in this biological suspension. It is noteworthy to note that it tends to maintain somewhat of its integrity even at higher volumes. Slight interactions between FBS and F127:H-[P(OEGMA-co-LMA)]=2 could be detected as no significant increase in hydrodynamic radii was recorded. On the other hand, the H-[P(OEGMA-co LMA)]:F127=1 is probably forming a large protein corona with serum proteins as a result of the increase in FBS. The addition of serum with a high protein diversity can be attributed to the rise in the PDI for all samples.

Regarding H-[P(OEGMA-co LMA)]:F127=1, 1:10 nanocarrier: FBS suspension and 1:9 FBS:PBS incubation experiment, it's likely that the nanocarrier coagulated with the proteins and produced nanostructures with greater mass, as indicated by the increase in intensity. This should cause the nanostructures to sediment. Additionally, a higher buffer concentration could cause the proteins to settle. The sample 1:1 nanocarrier: FBS suspension and 1:9 FBS:PBS with a higher protein suspension concentration. On the other hand, it fared better over time with no increase in volume or mass. This might be due to

the stronger interactions between the emerging structures and the serum proteins, which make them more stable.

In conclusion, both systems in the protein suspension form a protein corona. F127:H-[P(OEGMA-co-LMA)]=2. 1:1 nanocarrier: FBS suspension and 1:9 FBS:PBS produced the best results when no new peak at a larger value was recorded, indicating the nanocarrier has some stealth properties.

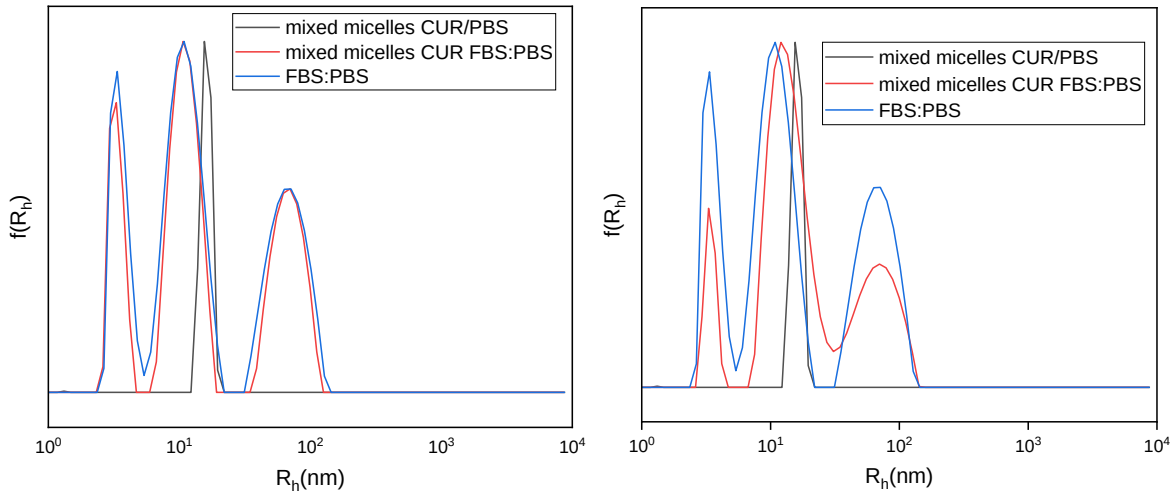

Figure 40. Ratio comparison of curcumin loaded mixed polymeric nanostructures H-[P(OEGMA-co LMA)]:F127=1, 1:10 nanocarrier: FBS suspension and 1:9 FBS:PBS (left) - 1:1 nanocarrier: FBS suspension and 1:9 FBS:PBS (right). Timeframe 1 hour.

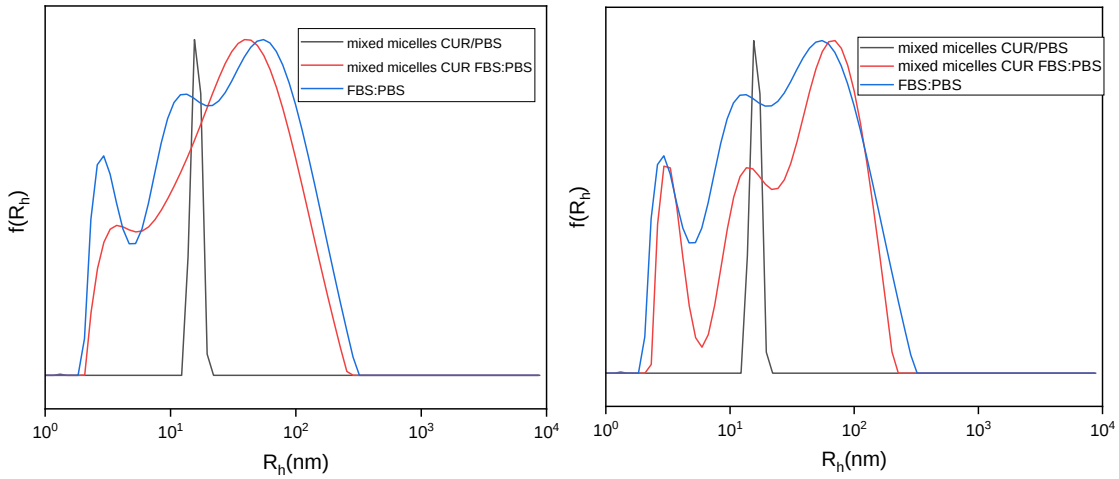

Figure 41. Ratio comparison of curcumin loaded mixed polymeric nanostructures H-[P(OEGMA-co LMA)]:F127=1, 1:1 nanocarrier: FBS suspension and 1:1 FBS:PBS (left) - 1:10 nanocarrier: FBS suspension and 1:1 FBS:PBS (right). Timeframe 1 hour.

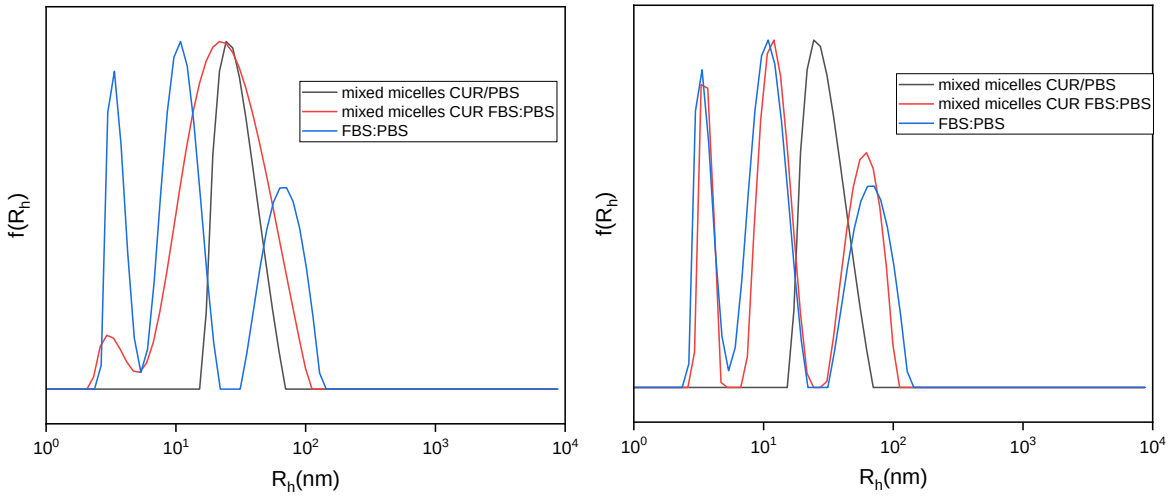

Figure 42. Ratio comparison of the curcumin-loaded mixed polymeric nanostructures F127:H-[P(OEGMA-co-LMA)]=2. 1:1 nanocarrier: FBS suspension and 1:9 FBS:PBS (left) - 1:10 nanocarrier: FBS suspension and 1:9 FBS:PBS (right), Timeframe 1 hour.

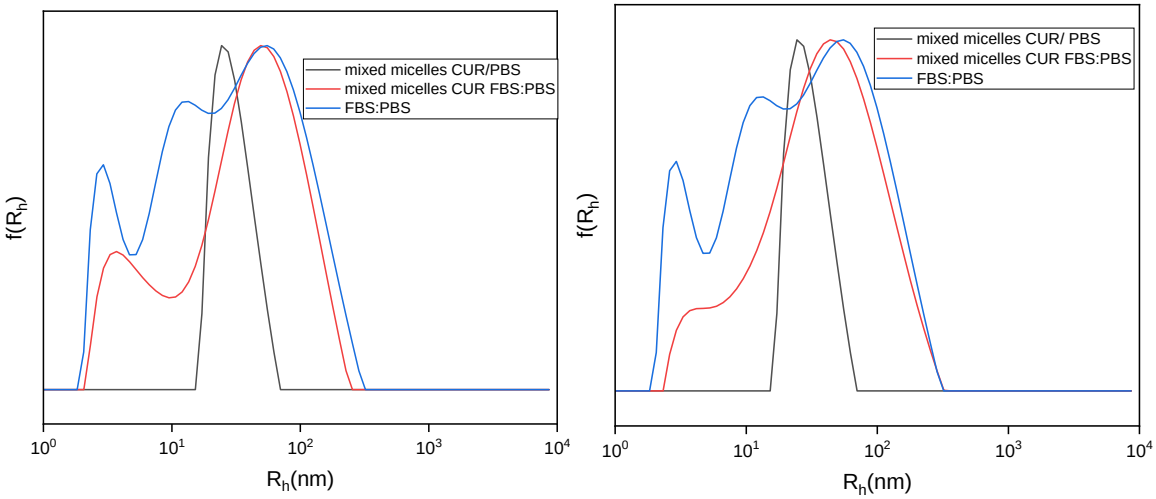

Figure 43. Ratio comparison of the curcumin-loaded mixed polymeric nanostructures F127:H-[P(OEGMA-co-LMA)]=2. 1:10 nanocarrier: FBS suspension and 1:9 FBS:PBS (left) - 1:1 nanocarrier: FBS suspension and 1:1 FBS:PBS (right), Timeframe 1 hour.

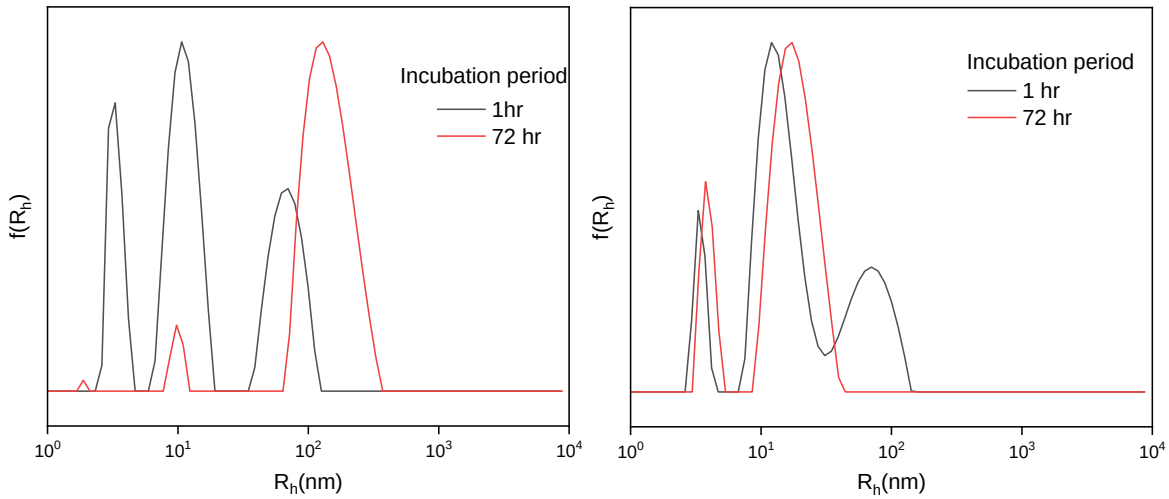

Figure 44. Ratio comparison of curcumin loaded mixed polymeric nanostructures H-[P(OEGMA-co LMA)]:F127=1, 1:10 nanocarrier: FBS suspension and 1:9 FBS:PBS (left) - 1:1 nanocarrier: FBS suspension and 1:9 FBS:PBS (right). Incubation period 72hr.

Sample	M:FBS (v:v)	FBS:PBS (v:v)	Rh (nm)	Intensity(A.U.)	PDI
H-[P(OEGMA-co LMA)]:F127=1,	1:10	1:9	3 11 69	540	0.471
	1:1	1:9	3 22	473	0.42
	1:1	1:1	25	532	0.502
	1:10	1:1	30	370	0.505
F127:H-[P(OEGMA-co-LMA)]=2	1:1	1:9	22	517	0.377
	1:10	1:9	59 12	595	0.459
	1:10	1:1	30	363	0.494
	1:1	1:1	35	670	0.483

Table 11. DLS results of curcumin loaded mixed polymeric nanostructures [M:FBS= nanocarrier: FBS suspension(v/v), FBS:PBS (v/v)]. Incubation period 1hr

Sample	M:FBS (v:v)	FBS:PBS (v:v)	Incubation period	Rh (nm)	Intensity(A.U.)	PDI
H-[P(OEGMA-co LMA)]:F127=1,	1:10	1:9	1hr	3 11 69	540	0.471
			72hr	156 12	1100	0.374
	1:1	1:9	1hr	3 22	473	0.42
			72 hr	4 22	490	0.402

Table 12. DLS results of curcumin loaded mixed polymeric nanostructures [M:FBS= nanocarrier: FBS suspension(v/v), FBS:PBS (v/v)].

4.6 Fourier transform infrared spectroscopy (FTIR) spectroscopy

IR spectroscopy is a valuable method for validating the effective encapsulation of the drug indomethacin. The graph below depicts the IR spectra of H-[P(OEGMA-co LMA)]:F127=1 nanostructures, both loaded and unloaded. Indomethacin was also analyzed for comparison. The stretching of the C-O-C ether group is indicated by the prominent peak at 1104 cm^{-1}. The functional group of C=O present in indomethacin is responsible for the prominent peak at 1700 cm^{-1}. The interactions between the excipient and the drug are to account for the variations in the range of 1550 to 1750 cm^{-1}. The prominent peak at 2889 cm^{-1} is associated with the C-H stretch, which is also visible in Pluronic's IR spectra. C-OH stretch is responsible for the large broad peak at 3209 cm^{-1}.[109–111]

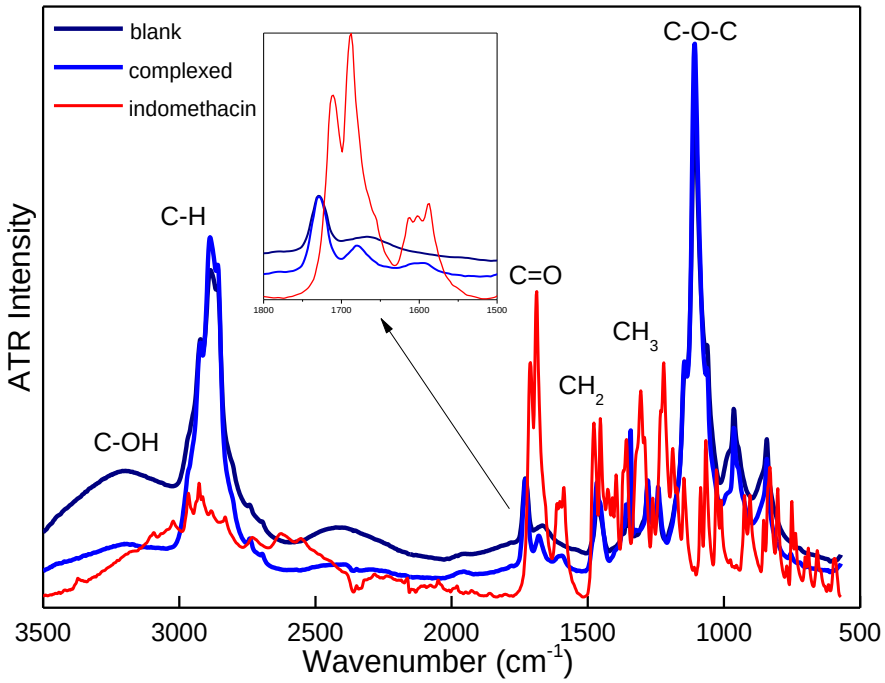

Figure 45. FTIR spectra of H-[P(OEGMA-co LMA)]:F127=1 unloaded, loaded, and indomethacin.

Conclusions

In our research, mixed copolymer-based nanocarriers, H-[P(OEGMA-co LMA)]:F127 were successfully prepared utilizing the thin film and co-solvent method. To investigate Pluronic's F127 behavior, two different ratios were implemented. Each approach succeeded in creating nanostructures, as demonstrated by the characterization of emerged systems utilizing dynamic light scattering. The co-solvent method produced nanocarriers with favorable attributes such as small average micelle hydrodynamic radius and low-size polydispersity indexes. All of the nanostructures formed using this simple technique did not surpass 50 nm, making them ideal candidates for drug delivery.

To be exact prepared unloaded mixed nanostructures exhibited R_h ranging from 14-20 nm above the rapid renal clearance cut-off value. The mixed nanostructures' CAC values were lower compared to aggregates generated under comparable circumstances from the precursor copolymers. The capability of the nanocarriers to encapsulate curcumin and indomethacin was examined, considering both the copolymer's biocompatibility and the satisfactory outcomes of the unloaded forms. Curcumin-loaded nanostructures exhibited Rh ranging from 17-29 nm. Curcumin loaded H-[P(OEGMA-co LMA)]:F127=1 almost achieved classification as a monodisperse suspension with a PDI value of 0.01.

It was discovered that all curcumin-loaded systems in PBS maintained their initial physicochemical properties over the 50 days. Nanosystems containing indomethacin required a longer time to settle in a more advantageous configuration. Indomethacin-loaded mixed systems were measured to be in the 19-31nm range, with polydispersity values ≤ 0.02.

It was established that the entrapment of hydrophobic substances in nanostructures aids in their vastly superior self-organization. The successful indomethacin encapsulation in the instance of H-[P(OEGMA-co LMA)]:F127=1 was further confirmed by IR spectra. In the region of 1550 to 1750 cm^{-1}, some interactions between the excipient and the drug were observed. Fluorescence spectroscopy was used to reveal whether curcumin's fluorescent properties persisted after encapsulation. The stability test utilizing dialysis and FS both demonstrated that indeed emerging systems have the potential to be employed in bioimaging.

To mimic the circumstances a nanoparticle might encounter in the bloodstream, curcumin-loaded nanostructures were analyzed in fetal bovine serum. In most cases, the mixed systems had strong interactions with the protein system forming a protein corona. F127:H-[P(OEGMA-co-LMA)]=2 performed the best.

This work only further adds to a growing corpus of research showing that mixed systems have the potential to outperform their parent copolymers. The main goal of mixed systems

is based on synergism, something that can be witnessed in the size, homogeneity, and CAC values of the emerged systems.

Discussion

This thesis objective was to produce mixed micelles from triblock Pluronic copolymer F127 and H-[P(OEGMA-co LMA)] hyperbranched copolymer that were loaded with indomethacin and curcumin, two poorly soluble drugs. The significant number and architecture of the hydrophobic sites in Pluronic F127 that can interact with hydrophobic drugs led to its selection over the other poloxamers. Poloxamers are also gaining popularity in the field of mixed micelles. H-[P(OEGMA-co LMA)] has hyperbranched units grouped randomly offering versatility. Both cooperate to achieve efficient self-assembly, which is due to the equilibrium between hydrophilic and hydrophobic units. Because of Pluronic's hydrophobicity, it is possible that larger hyperbranched copolymers will self-assemble into more numerous and compact nanostructures. The hyperbranched copolymer favors the combination with Pluronic as a protective measure in aqueous media. This is not a one-way street; the hyperbranched copolymer provides stability to the combined system.

Future research should consider other forms of biological media to evaluate the biocompatibility of the curcumin-loaded nanostructures. The stability of the indomethacin-loaded nanostructures will need to be further investigated in greater detail. Particularly to better evaluate protein interactions, such as in the case of curcumin. This experimental thesis provides a good starting point for discussion and further research in mixed systems.

Table of Abbreviations

API	Active Pharmaceutical Ingredient
CAC	Critical Aggregation Concentration
CMC	Critical Micelle Concentration
DLS	Dynamic Light Scattering
ELS	Electrophoretic Light Scattering
EPR	Enhanced Permeability and Retention Effect
FI	Fluorescence Imaging
FDA	Food and Drug Administration
FS	Fluorescence Spectroscopy
FT-IR	Fourier Transform Infrared Spectroscopy
FBS	Fetal Bovine Serum
ITC	Isothermal Titration Calorimetry
PPO	Poly(Propylene Oxide)
PEO	Poly(Ethylene Oxide)
PEG	Poly(Ethylene Glycol)
PBS	Phosphate Buffered Saline
PIC	Polyion Complex
PDI	Polydispersity Index
RAFT	Reversible Addition Fragmentation Chain Transfer

RES	Reticuloendothelial System
R_h	Hydrodynamic Radius
Solv. Evap	Co-solvent method
Uv-Vis	Ultraviolet–Visible
WFI	Water For Injection

References

1. Clarysse, S., Brouwers, J., Tack, J., Annaert, P. & Augustijns, P. Intestinal drug solubility estimation based on simulated intestinal fluids: Comparison with solubility in human intestinal fluids. *European Journal of Pharmaceutical Sciences* **43**, 260–269 (2011).
2. Liu, W. *et al.* Oral bioavailability of curcumin: problems and advancements. *J Drug Target* **24**, 694–702 (2016).
3. Cornelia Keck, Szymon Kobierski, Rachmat Mauludin & Rainer H. Müller. S ECOND GENERATION O F DRUG NANOCRYSTALS FOR DELIVERY O F POORLY SOLUBLE DRUGS : SMART C RYSTALS TECHNOLOGY. *D O S I S* (2008).
4. Ebrahim Attia, A. B. *et al.* Mixed micelles self-assembled from block copolymers for drug delivery. *Curr Opin Colloid Interface Sci* **16**, 182–194 (2011).
5. Basak, R. & Bandyopadhyay, R. Encapsulation of Hydrophobic Drugs in Pluronic F127 Micelles: Effects of Drug Hydrophobicity, Solution Temperature, and pH. *Langmuir* **29**, 4350–4356 (2013).
6. Gert Strobl. *The Physics of Polymers*. (Springer Berlin Heidelberg, 2007). doi:10.1007/978-3-540-68411-4.
7. Gerald Scott. Polymers and the Environment. (1999).
8. Wang, Y. & Grayson, S. M. Approaches for the preparation of non-linear amphiphilic polymers and their applications to drug delivery. *Adv Drug Deliv Rev* **64**, 852–865 (2012).
9. VELICHKOVA, R. Amphiphilic polymers from macromonomers and telechelics. *Prog Polym Sci* **20**, 819–887 (1995).
10. Zheng, W. & Wang, Z.-G. Morphology of ABC Triblock Copolymers. *Macromolecules* **28**, 7215–7223 (1995).
11. Konishcheva, E., Daubian, D., Gaitzsch, J. & Meier, W. Synthesis of Linear ABC Triblock Copolymers and Their Self-Assembly in Solution. *Helv Chim Acta* **101**, e1700287 (2018).
12. Ludwigs, S. *et al.* Self-assembly of functional nanostructures from ABC triblock copolymers. *Nat Mater* **2**, 744–747 (2003).
13. Hoang, N. H., Lim, C., Sim, T. & Oh, K. T. Triblock copolymers for nano-sized drug delivery systems. *J Pharm Investig* **47**, 27–35 (2017).
14. Hult, A., Johansson, M. & Malmström, E. Hyperbranched Polymers. in *Branched Polymers II* 1–34 (Springer Berlin Heidelberg). doi:10.1007/3-540-49780-3_1.
15. Gao, C. & Yan, D. Hyperbranched polymers: from synthesis to applications. *Prog Polym Sci* **29**, 183–275 (2004).
16. Hult, A., Johansson, M. & Malmström, E. Hyperbranched Polymers. in *Branched Polymers II* 1–34 (Springer Berlin Heidelberg). doi:10.1007/3-540-49780-3_1.
17. Voit, B. New developments in hyperbranched polymers. *J Polym Sci A Polym Chem* **38**, 2505–2525 (2000).
18. Svenson, S. The dendrimer paradox – high medical expectations but poor clinical translation. *Chem Soc Rev* **44**, 4131–4144 (2015).
19. Perrier, S. *50th Anniversary Perspective* : RAFT Polymerization—A User Guide. *Macromolecules* **50**, 7433–7447 (2017).
20. Hasirci, V., Yilgor, P., Endogan, T., Eke, G. & Hasirci, N. Polymer Fundamentals: Polymer Synthesis. in *Comprehensive Biomaterials* 349–371 (Elsevier, 2011). doi:10.1016/B978-0-08-055294-1.00034-9.

21. Truong, N. P., Jones, G. R., Bradford, K. G. E., Konkolewicz, D. & Anastasaki, A. A comparison of RAFT and ATRP methods for controlled radical polymerization. *Nat Rev Chem* **5**, 859–869 (2021).
22. Boyer, C. *et al.* Bioapplications of RAFT Polymerization. *Chem Rev* **109**, 5402–5436 (2009).
23. ΜΠΑΛΑΦΟΥΤΗ ΑΝΑΣΤΑΣΙΑ. Υπερδιακλαδισμένα Τυχαία Αμφίφιλα Συμπολυμερή Η-[P(OEGMA-co-LMA)]:Σύνθεση, Χαρακτηρισμός, Ιδιότητες σε διαλύματα και Δυνατότητα εγκλωβισμού υδρόφοβων ενώσεων. (2021).
24. Qian, J., Xu, W., Zhang, W. & Jin, X. Preparation and characterization of biomorphic poly(l-lactide-co-β-malic acid) scaffolds. *Mater Lett* **124**, 313–317 (2014).
25. Bohorquez, M., Koch, C., Trygstad, T. & Pandit, N. A Study of the Temperature-Dependent Micellization of Pluronic F127. *J Colloid Interface Sci* **216**, 34–40 (1999).
26. Chen, S., Pieper, R., Webster, D. C. & Singh, J. Triblock copolymers: synthesis, characterization, and delivery of a model protein. *Int J Pharm* **288**, 207–218 (2005).
27. Khattak, S. F., Bhatia, S. R. & Roberts, S. C. Pluronic F127 as a Cell Encapsulation Material: Utilization of Membrane-Stabilizing Agents. *Tissue Eng* **11**, 974–983 (2005).
28. al Khateb, K. *et al.* In situ gelling systems based on Pluronic F127/Pluronic F68 formulations for ocular drug delivery. *Int J Pharm* **502**, 70–79 (2016).
29. Desai, S. D. & Blanchard, J. In Vitro Evaluation of Pluronic F127-Based Controlled-Release Ocular Delivery Systems for Pilocarpine. *J Pharm Sci* **87**, 226–230 (1998).
30. Basak, R. & Bandyopadhyay, R. Encapsulation of Hydrophobic Drugs in Pluronic F127 Micelles: Effects of Drug Hydrophobicity, Solution Temperature, and pH. *Langmuir* **29**, 4350–4356 (2013).
31. Sharma, P. K. & Bhatia, S. R. Effect of anti-inflammatories on Pluronic® F127: micellar assembly, gelation and partitioning. *Int J Pharm* **278**, 361–377 (2004).
32. Akash, M. S. H., Rehman, K. & Chen, S. Pluronic F127-Based Thermosensitive Gels for Delivery of Therapeutic Proteins and Peptides. *Polymer Reviews* **54**, 573–597 (2014).
33. Talelli, M. & Hennink, W. E. Thermosensitive polymeric micelles for targeted drug delivery. *Nanomedicine* **6**, 1245–1255 (2011).
34. Bermejo, M., Sanchez-Dengra, B., Gonzalez-Alvarez, M. & Gonzalez-Alvarez, I. Oral controlled release dosage forms: dissolution versus diffusion. *Expert Opin Drug Deliv* **17**, 791–803 (2020).
35. Saxena, V. & Hussain, M. D. Polymeric Mixed Micelles for Delivery of Curcumin to Multidrug Resistant Ovarian Cancer. *J Biomed Nanotechnol* **9**, 1146–1154 (2013).
36. Cabral, H., Miyata, K., Osada, K. & Kataoka, K. Block Copolymer Micelles in Nanomedicine Applications. *Chem Rev* **118**, 6844–6892 (2018).
37. Pepić, I., Lovrić, J. & Filipović-Grčić, J. How do polymeric micelles cross epithelial barriers? *European Journal of Pharmaceutical Sciences* **50**, 42–55 (2013).
38. Parra, A., Jarak, I., Santos, A., Veiga, F. & Figueiras, A. Polymeric Micelles: A Promising Pathway for Dermal Drug Delivery. *Materials* **14**, 7278 (2021).
39. Kwon, G. S. & Okano, T. Polymeric micelles as new drug carriers. *Adv Drug Deliv Rev* **21**, 107–116 (1996).
40. Aliabadi, H. M. & Lavasanifar, A. Polymeric micelles for drug delivery. *Expert Opin Drug Deliv* **3**, 139–162 (2006).
41. Miyata, K., Christie, R. J. & Kataoka, K. Polymeric micelles for nano-scale drug delivery. *React Funct Polym* **71**, 227–234 (2011).

42. Ahmad, Z., Shah, A., Siddiq, M. & Kraatz, H.-B. Polymeric micelles as drug delivery vehicles. *RSC Adv.* **4**, 17028–17038 (2014).
43. Torchilin, V. Tumor delivery of macromolecular drugs based on the EPR effect. *Adv Drug Deliv Rev* **63**, 131–135 (2011).
44. Stylianopoulos, T. EPR-effect: utilizing size-dependent nanoparticle delivery to solid tumors. *Ther Deliv* **4**, 421–423 (2013).
45. Vollrath, A., Schubert, S. & Schubert, U. S. Fluorescence imaging of cancer tissue based on metal-free polymeric nanoparticles – a review. *J Mater Chem B* **1**, 1994 (2013).
46. Gyawali, D. *et al.* Fluorescence Imaging Enabled Biodegradable Photostable Polymeric Micelles. *Adv Healthc Mater* **3**, 182–186 (2014).
47. Wolfbeis, O. S. An overview of nanoparticles commonly used in fluorescent bioimaging. *Chem Soc Rev* **44**, 4743–4768 (2015).
48. Ruedas-Rama, M. J., Walters, J. D., Orte, A. & Hall, E. A. H. Fluorescent nanoparticles for intracellular sensing: A review. *Anal Chim Acta* **751**, 1–23 (2012).
49. Li, K. & Liu, B. Polymer-encapsulated organic nanoparticles for fluorescence and photoacoustic imaging. *Chem. Soc. Rev.* **43**, 6570–6597 (2014).
50. Manjappa, A. S., Kumbhar, P. S., Patil, A. B., Disouza, J. I. & Patravale, V. B. Polymeric Mixed Micelles: Improving the Anticancer Efficacy of Single-Copolymer Micelles. *Crit Rev Ther Drug Carrier Syst* **36**, 1–58 (2019).
51. Wakebayashi, D. *et al.* Lactose-conjugated polyion complex micelles incorporating plasmid DNA as a targetable gene vector system: their preparation and gene transfecting efficiency against cultured HepG2 cells. *Journal of Controlled Release* **95**, 653–664 (2004).
52. Ebrahim Attia, A. B. *et al.* Mixed micelles self-assembled from block copolymers for drug delivery. *Curr Opin Colloid Interface Sci* **16**, 182–194 (2011).
53. Cagel, M. *et al.* Polymeric mixed micelles as nanomedicines: Achievements and perspectives. *European Journal of Pharmaceutics and Biopharmaceutics* **113**, 211–228 (2017).
54. Leung, M. H. M., Colangelo, H. & Kee, T. W. Encapsulation of Curcumin in Cationic Micelles Suppresses Alkaline Hydrolysis. *Langmuir* **24**, 5672–5675 (2008).
55. Hagl, S. *et al.* Curcumin micelles improve mitochondrial function in neuronal PC12 cells and brains of NMRI mice – Impact on bioavailability. *Neurochem Int* **89**, 234–242 (2015).
56. Esatbeyoglu, T. *et al.* Curcumin-From Molecule to Biological Function. *Angewandte Chemie International Edition* **51**, 5308–5332 (2012).
57. Liu, W. *et al.* Oral bioavailability of curcumin: problems and advancements. *J Drug Target* **24**, 694–702 (2016).
58. Yang, R. *et al.* Biodegradable Polymer-Curcumin Conjugate Micelles Enhance the Loading and Delivery of Low-Potency Curcumin. *Pharm Res* **29**, 3512–3525 (2012).
59. Zhao, L. *et al.* Curcumin loaded mixed micelles composed of Pluronic P123 and F68: Preparation, optimization and in vitro characterization. *Colloids Surf B Biointerfaces* **97**, 101–108 (2012).
60. Sahu, A., Kasoju, N., Goswami, P. & Bora, U. Encapsulation of Curcumin in Pluronic Block Copolymer Micelles for Drug Delivery Applications. *J Biomater Appl* **25**, 619–639 (2011).
61. Gyun Shin, I., Yeon Kim, S., Moo Lee, Y., Soo Cho, C. & Yong Kiel Sung. Methoxy poly(ethylene glycol)/ϵ-caprolactone amphiphilic block copolymeric micelle containing indomethacin. *Journal of Controlled Release* **51**, 1–11 (1998).

62. Lucas, S. The Pharmacology of Indomethacin. *Headache: The Journal of Head and Face Pain* **56**, 436–446 (2016).
63. Maity, B., Chatterjee, A., Ahmed, S. A. & Seth, D. Interaction of the Nonsteroidal Anti-inflammatory Drug Indomethacin with Micelles and Its Release. *J Phys Chem B* **119**, 3776–3785 (2015).
64. La, S. B., Okano, T. & Kataoka, K. Preparation and Characterization of the Micelle-Forming Polymeric Drug Indomethacin-Incorporated Polyfethylene oxide)-Poly(β-benzyl L-aspartate) Block Copolymer Micelles. *J Pharm Sci* **85**, 85–90 (1996).
65. Park, K. M., Bae, J. W., Joung, Y. K., Shin, J. W. & Park, K. D. Nanoaggregate of thermosensitive chitosan-Pluronic for sustained release of hydrophobic drug. *Colloids Surf B Biointerfaces* **63**, 1–6 (2008).
66. Zhang, J. X. *et al.* Local Delivery of Indomethacin to Arthritis-Bearing Rats through Polymeric Micelles Based on Amphiphilic Polyphosphazenes. *Pharm Res* **24**, 1944–1953 (2007).
67. Malvern Instruments Ltd. Dynamic Light Scattering: An Introduction in 30 Minutes .
68. Stetefeld, J., McKenna, S. A. & Patel, T. R. Dynamic light scattering: a practical guide and applications in biomedical sciences. *Biophys Rev* **8**, 409–427 (2016).
69. Kaszuba, M., McKnight, D., Connah, M. T., McNeil-Watson, F. K. & Nobbmann, U. Measuring sub nanometre sizes using dynamic light scattering. *Journal of Nanoparticle Research* **10**, 823–829 (2008).
70. Dandong Bettersize Instruments Ltd. Dynamic Light Scattering (DLS). *environmental-expert* (2019).
71. Clogston, J. D. & Patri, A. K. Zeta Potential Measurement. in 63–70 (2011). doi:10.1007/978-1-60327-198-1_6.
72. z potential theory. *Manual: Zetasizer Nano User Manual*.
73. Justin Tom, P. UV-Vis Spectroscopy: Principle, Strengths and Limitations and Applications. *Technology Networks* (2021).
74. Deshbandhu College, U. of D. UV-Vis Spectroscopy.
75. Pavan M. V. Raja & Andrew R. Barron. UV-Visible Spectroscopy. *Libretexts*.
76. Richard Osibanjo, Rachael Curtis & Zijuan Lai. Infrared Spectroscopy. *Libretexts*.
77. Dyamenahalli, K., Famili, A. & Shandas, R. Characterization of shape-memory polymers for biomedical applications. in *Shape Memory Polymers for Biomedical Applications* 35–63 (Elsevier, 2015). doi:10.1016/B978-0-85709-698-2.00003-9.
78. Mohamed, M. A., Jaafar, J., Ismail, A. F., Othman, M. H. D. & Rahman, M. A. Fourier Transform Infrared (FTIR) Spectroscopy. in *Membrane Characterization* 3–29 (Elsevier, 2017). doi:10.1016/B978-0-444-63776-5.00001-2.
79. Masuda, H., Takenaka, Y., Yamaguchi, A., Nishikawa, S. & Mizuno, H. A novel yellowish-green fluorescent protein from the marine copepod, Chiridius poppei, and its use as a reporter protein in HeLa cells. *Gene* **372**, 18–25 (2006).
80. Nguyen, H. N. *et al.* Curcumin as fluorescent probe for directly monitoring *in vitro* uptake of curcumin combined paclitaxel loaded PLA-TPGS nanoparticles. *Advances in Natural Sciences: Nanoscience and Nanotechnology* **7**, 025001 (2016).
81. *Principles of Fluorescence Spectroscopy*. (Springer US, 2006). doi:10.1007/978-0-387-46312-4.
82. Royer, C. A. Approaches to teaching fluorescence spectroscopy. *Biophys J* **68**, 1191–1195 (1995).

83. Π.Χ. ΙΩΑΝΝΟΥ. ΣΗΜΕΙΩΣΕΙΣ ΜΕΤΑΠΤΥΧΙΑΚΟΥ ΜΑΘΗΜΑΤΟΣ “ΠΡΟΧΩΡΗΜΕΝΗ ΑΝΑΛΥΤΙΚΗ ΧΗΜΕΙΑ”.

84. Fang, X. *et al.* Pluronic P105/F127 mixed micelles for the delivery of docetaxel against Taxol-resistant non-small cell lung cancer: optimization and in vitro, in vivo evaluation. *Int J Nanomedicine* 73 (2013) doi:10.2147/IJN.S38221.

85. Lu, Y., Zhang, E., Yang, J. & Cao, Z. Strategies to improve micelle stability for drug delivery. *Nano Res* **11**, 4985–4998 (2018).

86. Hwang, D., Ramsey, J. D. & Kabanov, A. v. Polymeric micelles for the delivery of poorly soluble drugs: From nanoformulation to clinical approval. *Adv Drug Deliv Rev* **156**, 80–118 (2020).

87. Kabanov, A. v. *et al.* Micelle Formation and Solubilization of Fluorescent Probes in Poly(oxyethylene-b-oxypropylene-b-oxyethylene) Solutions. *Macromolecules* **28**, 2303–2314 (1995).

88. Sharma, R. & Sharma, S. *Physiology, Blood Volume*. (2022).

89. Bhattacharjee, S. DLS and zeta potential – What they are and what they are not? *Journal of Controlled Release* **235**, 337–351 (2016).

90. Le-Vinh, B., Le, N.-M. N., Nazir, I., Matuszczak, B. & Bernkop-Schnürch, A. Chitosan based micelle with zeta potential changing property for effective mucosal drug delivery. *Int J Biol Macromol* **133**, 647–655 (2019).

91. Halder, S. *et al.* Alteration of Zeta potential and membrane permeability in bacteria: a study with cationic agents. *Springerplus* **4**, 672 (2015).

92. Basak, R. & Bandyopadhyay, R. Encapsulation of Hydrophobic Drugs in Pluronic F127 Micelles: Effects of Drug Hydrophobicity, Solution Temperature, and pH. *Langmuir* **29**, 4350–4356 (2013).

93. Dantas Lopes dos Santos, D. *et al.* Curcumin-loaded Pluronic ® F-127 Micelles as a Drug Delivery System for Curcumin-mediated Photodynamic Therapy for Oral Application. *Photochem Photobiol* **97**, 1072–1088 (2021).

94. Sahu, A., Kasoju, N., Goswami, P. & Bora, U. Encapsulation of Curcumin in Pluronic Block Copolymer Micelles for Drug Delivery Applications. *J Biomater Appl* **25**, 619–639 (2011).

95. Kouchakzadeh, H., Shojaosadati, S. A., Maghsoudi, A. & Vasheghani Farahani, E. Optimization of PEGylation Conditions for BSA Nanoparticles Using Response Surface Methodology. *AAPS PharmSciTech* **11**, 1206–1211 (2010).

96. Nel, A. E. *et al.* Understanding biophysicochemical interactions at the nano–bio interface. *Nat Mater* **8**, 543–557 (2009).

97. Kumar, P., Kandi, S. K., Manohar, S., Mukhopadhyay, K. & Rawat, D. S. Monocarbonyl Curcuminoids with Improved Stability as Antibacterial Agents against *Staphylococcus aureus* and Their Mechanistic Studies. *ACS Omega* **4**, 675–687 (2019).

98. Govindaraju, S., Rengaraj, A., Arivazhagan, R., Huh, Y.-S. & Yun, K. Curcumin-Conjugated Gold Clusters for Bioimaging and Anticancer Applications. *Bioconjug Chem* **29**, 363–370 (2018).

99. Liu, H., Farrell, S. & Uhrich, K. Drug release characteristics of unimolecular polymeric micelles. *Journal of Controlled Release* **68**, 167–174 (2000).

100. Yu, M., Yuan, W., Li, D., Schwendeman, A. & Schwendeman, S. P. Predicting drug release kinetics from nanocarriers inside dialysis bags. *Journal of Controlled Release* **315**, 23–30 (2019).

101. Leo, E., Cameroni, R. & Forni, F. Dynamic dialysis for the drug release evaluation from doxorubicin–gelatin nanoparticle conjugates. *Int J Pharm* **180**, 23–30 (1999).
102. D'Souza, S. A Review of *In Vitro* Drug Release Test Methods for Nano-Sized Dosage Forms. *Advances in Pharmaceutics* **2014**, 1–12 (2014).
103. Selianitis, D. & Pispas, S. P(<scp> MMA- *co* -HPMA </scp>)- <scp> *b* -POEGMA </scp> copolymers: synthesis, micelle formation in aqueous media and drug encapsulation. *Polym Int* **70**, 1508–1522 (2021).
104. Gstraunthaler, G., Lindl, T. & van der Valk, J. A plea to reduce or replace fetal bovine serum in cell culture media. *Cytotechnology* **65**, 791–793 (2013).
105. Ha, Y., Wang, X., Liljestrand, H. M., Maynard, J. A. & Katz, L. E. Bioavailability of Fullerene under Environmentally Relevant Conditions: Effects of Humic Acid and Fetal Bovine Serum on Accumulation in Lipid Bilayers and Cellular Uptake. *Environ Sci Technol* **50**, 6717–6727 (2016).
106. Wiogo, H. T. R., Lim, M., Bulmus, V., Yun, J. & Amal, R. Stabilization of Magnetic Iron Oxide Nanoparticles in Biological Media by Fetal Bovine Serum (FBS). *Langmuir* **27**, 843–850 (2011).
107. Pippa, N., Kaditi, E., Pispas, S. & Demetzos, C. PEO-b-PCL–DPPC chimeric nanocarriers: self-assembly aspects in aqueous and biological media and drug incorporation. *Soft Matter* **9**, 4073 (2013).
108. Chroni, A., Mavromoustakos, T. & Pispas, S. Poly(2-oxazoline)-Based Amphiphilic Gradient Copolymers as Nanocarriers for Losartan: Insights into Drug–Polymer Interactions. *Macromol* **1**, 177–200 (2021).
109. Karolewicz, B., Gajda, M., Górniak, A., Owczarek, A. & Mucha, I. Pluronic F127 as a suitable carrier for preparing the imatinib base solid dispersions and its potential in development of a modified release dosage forms. *J Therm Anal Calorim* **130**, 383–390 (2017).
110. Kafetzi, M., Pispas, S., Bao, X. & Yao, P. Amphiphilic QP(DMAEMA-co-LMA)-b-POEGMA Random-Block Terpolymers as Nanocarriers for Insulin. *Biomedicines* **8**, 392 (2020).
111. Jain, D. K., Darwhekar, G., Solanki, S. S. & Sharma, R. Osmotically regulated asymmetric capsular system for sustained delivery of indomethacin. *J Pharm Investig* **43**, 27–35 (2013).